nature communications

Article

https://doi.org/10.1038/s41467-024-50964-z

A neurodevelopmental disorder mutation locks G proteins in the transitory pre-activated state

Received: 5 October 2023

Accepted: 25 July 2024

Published online: 05 August 2024

Check for updates

Kevin M. Knight[1,8,9], Brian E. Krumm[1,9], Nicholas J. Kapolka[1], W. Grant Ludlam[2], Meng Cui[3], Sepehr Mani[3], Iya Prytkova[4], Elizabeth G. Obarow[1], Tyler J. Lefevre[5], Wenyuan Wei[6], Ning Ma[6], Xi-Ping Huang[1], Jonathan F. Fay[7], Nagarajan Vaidehi[6], Alan V. Smrcka[5], Paul A. Slesinger[4], Diomedes E. Logothetis[3], Kirill A. Martemyanov[2], Bryan L. Roth[1] & Henrik G. Dohlman[1]

Many neurotransmitter receptors activate G proteins through exchange of GDP for GTP. The intermediate nucleotide-free state has eluded characterization, due largely to its inherent instability. Here we characterize a G protein variant associated with a rare neurological disorder in humans. $G\alpha_o^{K46E}$ has a charge reversal that clashes with the phosphate groups of GDP and GTP. As anticipated, the purified protein binds poorly to guanine nucleotides yet retains wild-type affinity for G protein βγ subunits. In cells with physiological concentrations of nucleotide, $G\alpha_o^{K46E}$ forms a stable complex with receptors and Gβγ, impeding effector activation. Further, we demonstrate that the mutant can be easily purified in complex with dopamine-bound D2 receptors, and use cryo-electron microscopy to determine the structure, including both domains of $G\alpha_o$, without nucleotide or stabilizing nanobodies. These findings reveal the molecular basis for the first committed step of G protein activation, establish a mechanistic basis for a neurological disorder, provide a simplified strategy to determine receptor-G protein structures, and a method to detect high affinity agonist binding in cells.

Many clinically important drugs, environmental signals, hormones, and neurotransmitters elicit their effects through G protein-coupled receptors (GPCRs). Receptors of this class represent one of the largest gene families, and by far the largest class of drug targets, and includes members with little or no shared sequence similarity. In contrast, G proteins are highly conserved in structure and function, and in mammals consist of just four subfamilies (G_s, $G_{i/o}$, $G_{q/11}$, and $G_{12/13}$) encoded by 16 individual genes.

The ability of such widely divergent receptors to activate a comparatively small number of G proteins indicates a shared mechanism of activation[1,2]. Broadly speaking, agonist binding to receptors leads to conformational changes in the G protein α subunit, release of GDP,

[1]Department of Pharmacology, University of North Carolina at Chapel Hill, Chapel Hill, NC, USA. [2]Department of Neuroscience, The Herbert Wertheim UF Scripps Institute for Biomedical Innovation & Technology, University of Florida, Jupiter, FL, USA. [3]Department of Pharmaceutical Sciences Northeastern University, Boston, MA, USA. [4]Nash Family Department of Neuroscience, Icahn School of Medicine at Mount Sinai, New York, NY, USA. [5]Department of Pharmacology, University of Michigan, Ann Arbor, MI, USA. [6]Department of Computational and Quantitative Medicine, Beckman Research Institute of the City of Hope, Duarte, CA, USA. [7]Department of Biochemistry and Molecular Biology, School of Medicine, University of Maryland, Baltimore, Baltimore, MD, USA. [8]Present address: Department of Neuroscience, The Herbert Wertheim UF Scripps Institute for Biomedical Innovation & Technology, University of Florida, Jupiter, FL, USA. [9]These authors contributed equally: Kevin M. Knight, Brian E. Krumm. e-mail: hdohlman@med.unc.edu

binding to GTP, and dissociation of Gα-GTP from the Gβγ dimer[3,4]. Either of the dissociated subunits can modulate the activity of downstream effector proteins, including adenylyl cyclase and phospholipase Cβ[5,6], among others. In addition, Gβγ dimers regulate potassium channels, calcium channels, phosphatidylinositol 3-kinases and MAPKs[7]. Agonist-induced signaling is terminated after Gα hydrolyzes GTP and the subunits reassemble; in most cases, this inactivation step is accelerated by regulators of G protein signaling (RGS) proteins[3]. Thus, receptors serve as signal discriminators and nucleotide exchange factors, RGS proteins serve as timing devices and G proteins serve as determinants of output specificity.

Activated GPCRs can stabilize the G protein in the nucleotide-free (apo) state, thereby facilitating GTP-GDP exchange[8–10]. The G protein nucleotide exchange step is likely accomplished by opening the cleft between the two domains of a given Gα protein in conjunction with docking of the α5 helix to the receptor[11,12]. Direct evidence of such inter-domain movement was first provided through double electron-electron resonance experiments on rhodopsin-activated $G\alpha_i$[13] and $G\alpha_s$[14], as well as through hydrogen-deuterium exchange studies[15,16], and X-ray crystallographic studies of the β_2-adrenergic receptor bound to the G_s protein heterotrimer[17]. In every study, Gβγ remained associated with Gα in the apo state. However, upon binding to GTP, the G protein subunits dissociate and are free to activate downstream effectors. Thus, the process of G protein activation is comprised of three discrete binding and unbinding transformations: (*i*) GPCR-dependent unbinding of GDP and stabilization of the nucleotide-free form of Gα, (*ii*) GTP-binding-dependent conformational changes in Gα, and (*iii*) unbinding of Gα-GTP from the Gβγ subunits (Fig. 1A).

Previous studies have characterized mutations that disrupt each of the transformations.

Lambert and colleagues described two types of Gα mutants[18,19], both of which bind stably with agonist-occupied receptor but fail to release GDP[20]. One strategy involved inserting four amino acids and extending the α5 helix, mimicking the translation that normally occurs during receptor engagement. Under these circumstances receptor-G protein subtype selectivity was diminished[20]. Mutations at the catalytic glutamine (required for GTP hydrolysis[21,22]) impose an ensemble of activated states that lead to sustained effector activation[23]. Mutations at a conserved arginine, part of the Gly-Arg-Glu (G-R-E) triad, prevent the release of Gβγ even in the GTP-bound state (Fig. 1A)[24].

Following a recent comprehensive screen of mutations associated with a neurological disorder in humans[25], we identified a substitution ($G\alpha_o^{K46E}$) that seemed likely to prevent guanine nucleotide binding, and thereby impose the first transformation state of the activation process (Fig. 1A)[26,27]. Of the 55 mutations tested, $G\alpha_o^{K46E}$ most strongly suppressed signaling in cells. This phosphate-interacting and neutralizing Lys ("pinK") is conserved in all G proteins (Fig. 1B), as well as in most protein kinases[28]. By swapping a positively charged side chain with one that is negatively charged, and at a position buried within the nucleotide-binding pocket, the Lys-to-Glu ("pinKE") substitution is likely to repel the phosphate groups of GDP and GTP (Fig. 1C, D). At the same time, the presence of the glutamate may help to secure the protein in the apo state, since the negatively charged residue may take the place of the negatively charged phosphates.

Here, we demonstrate that the pinKE mutation is incompatible with proper nucleotide binding but preserves the ability of the protein to bind receptors and Gβγ, as determined through detailed protein structure and function analysis. Consequently, this mutant inhibits signaling, in a dominant-negative fashion, as determined through cell-based activity measures. Our investigations reveal a likely mechanism of action for a rare neurological disorder and provide a tool for the isolation and characterization of G proteins in complex with agonist-occupied receptors.

Results

Dominant negative inhibition of Gβγ signaling

In a screen of 55 $G\alpha_o$ mutations, each associated with a neurological disorder in humans[25], we identified a subset of 29 mutations that suppress Gβγ dissociation in cells. Because these mutants inhibit signaling in the presence of wild-type Gα, they may be regarded as dominant negative mutants[29,30]. Of the 55 variants tested, the best-performing mutant had a charge substitution at a conserved lysine that bridges the β and γ phosphates of GTP. Replacement of the lysine with a negatively charged glutamate ($G\alpha_o^{K46E}$) is likely to be incompatible with GDP or GTP binding, due to charge-charge repulsion. Therefore, we postulated that $G\alpha_o^{K46E}$ persists in the nucleotide-free state and, consequently, remains associated with Gβγ and receptor. To test this hypothesis, we used bioluminescence resonance energy transfer (BRET) to monitor Gα-Rluc8 dissociation from Gβγ-GFP2 following GPCR activation (Fig. 2A)[25,31]. Lys46 is conserved in all human Gα members (position G.H1.01 using the CGN nomenclature[1]; Fig. 1B). To determine if its function is conserved, we introduced pinKE mutations into 10 human Gα-Rluc8 subtypes and the two major splice variants of $G\alpha_o$. As controls we used wild-type Gα-Rluc and a mutation at a conserved arginine (triadRC, position G.H2.04)[27,32,33], which is necessary for GTP-dependent subunit dissociation[24]. We co-transfected HEK293T cells with these G protein variants and with canonical receptors known to couple to each subtype; the μ-opioid receptor (MOR, couples to $G\alpha_{i1}$, $G\alpha_{i2}$, $G\alpha_{i3}$, $G\alpha_z$, $G\alpha_{oA}$, and $G\alpha_{oB}$), the dopamine D_2 receptor (D2R, couples to $G\alpha_{oA}$ and $G\alpha_{oB}$), the neurotensin 1 receptor (NT1R, couples to $G\alpha_q$, $G\alpha_{11}$, $G\alpha_{13}$ and $G\alpha_{15}$), and the β_2-adrenergic receptor (β_2AR, couples to $G\alpha_s$) (Supplementary Fig. 1)[31]. For all ten subtypes tested, the triadRC substitutions led to diminished subunit dissociation (Fig. 2A and Supplementary Fig. 1A), consistent with the known defect in GTP-dependent conformational changes[24]. The pinKE substitutions likewise diminished responses (Fig. 2A and Supplementary Fig. 1A, B). Notably, a subset of pinKE mutants displayed significantly reduced luminescence, basal BRET ratios, or both, indicating poor expression or association, respectively (Supplementary Fig. 1C and 1D). While $G\alpha_{oA}$ appeared to express more poorly than the other subtypes tested (Supplementary Fig. 1C), it bound particularly well to Gβγ under basal conditions (Supplementary Fig. 1D). Together, these data indicate that Lys46 is needed for proper Gβγ dissociation.

The BRET method used above provides a direct and quantitative readout of distance between donor and acceptor, in this case bound to Gα and Gβγ, and therefore is well suited for comparison of the pinKE substitutions in multiple Gα subtypes. Using this method, we demonstrated that pinKE impedes the release of Gβγ [25], in the manner of the triad arginine mutant[24]. Whereas the triadRC mutant assembles with Gβγ even in the GTP-bound state, however, we postulated that pinKE would be predominantly in the nucleotide-free state and would thus fail to dissociate from receptors as well as from Gβγ.

While the diminished BRET signal can reflect diminished proximity, it is also dependent on the dipole angle of the fluorophores within each Gα subtype. In addition, it is possible that some G proteins do not fully dissociate following receptor activation. As an additional test of our hypothesis, we used an alternative BRET method, one that measures the ability of the mutant to inhibit receptor-mediated activation and in competition with wild-type G protein. Once again, we compared the response to dopamine as well as to μ-opioid ligands, but in this case we monitored the ability of free Gβγ to bind the C-terminal domain of the G protein-coupled receptor kinase (GRK3ct)[34–36]. As shown in Fig. 2B, wild type - but not the pinKE mutant – form of $G\alpha_{oA}$ (hereafter $G\alpha_o$) released Gβγ in response to agonists, as indicated by the relative increase in fluorescence over time. We then tested the ability of pinKE to suppress signaling by wild-type $G\alpha_o$, coexpressed in the same cell. As shown in Fig. 2C, an extra copy of $G\alpha_o$ dampened the

https://doi.org/10.1038/s41467-024-50964-z

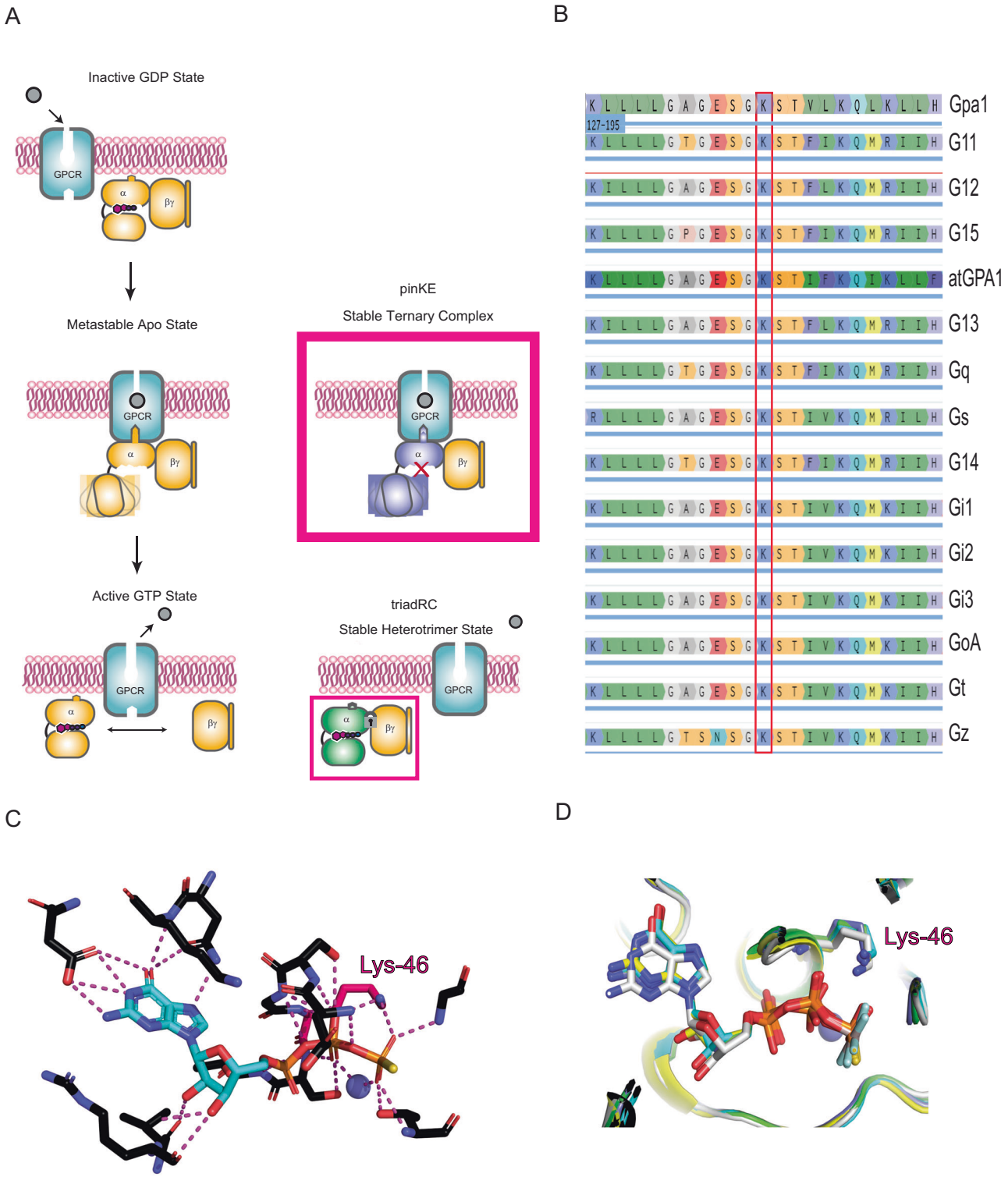

Fig. 1 | The phosphate-interacting and neutralizing lysine (pinK) controls one of three binding and unbinding transformations in Gα. A Agonist binding leads to stabilization of the nucleotide-free form of the G protein heterotrimer, while GTP binding leads to conformational changes in Gα and unbinding of Gα-GTP from the Gβγ subunits. Mutations disrupt GTP binding (pinKE) and GTP-dependent subunit dissociation (triadRC). **B** The conserved phosphate interacting and neutralizing lysine (pinK) is present in all human Gα proteins as well as Gα proteins from the yeast *S. cerevisiae* (Gpa1) and plant *A. thaliana* (AtGPA1). **C** pinK (Lys-46 in $G\alpha_o$) forms polar interactions with GTP. **D** Overlay of multiple Gα structures from PDB ID: 1GIA (G_{i1}, green), 1AZT (G_s, cyan), 1TND (G_t, blue), 3C7K (G_o, gray), and 1ZCA (G_{12}, yellow), showing that pinK bridges the β and γ phosphates of GTP.

response while pinKE largely abrogated the response (see also Supplementary Fig. 1E). Thus, and as anticipated by our model, $G\alpha_o^{K46E}$ suppressed the release of Gβγ, and did so both in the absence and presence of wild-type $G\alpha_o$.

The results shown above indicate that $G\alpha_o^{K46E}$ forms a non-productive complex with Gβγ. Our model was that it also binds stably to agonist-bound receptors, and by extension with Gβγ. To test this feature of the model we used another protein proximity assay, one that

https://doi.org/10.1038/s41467-024-50964-z

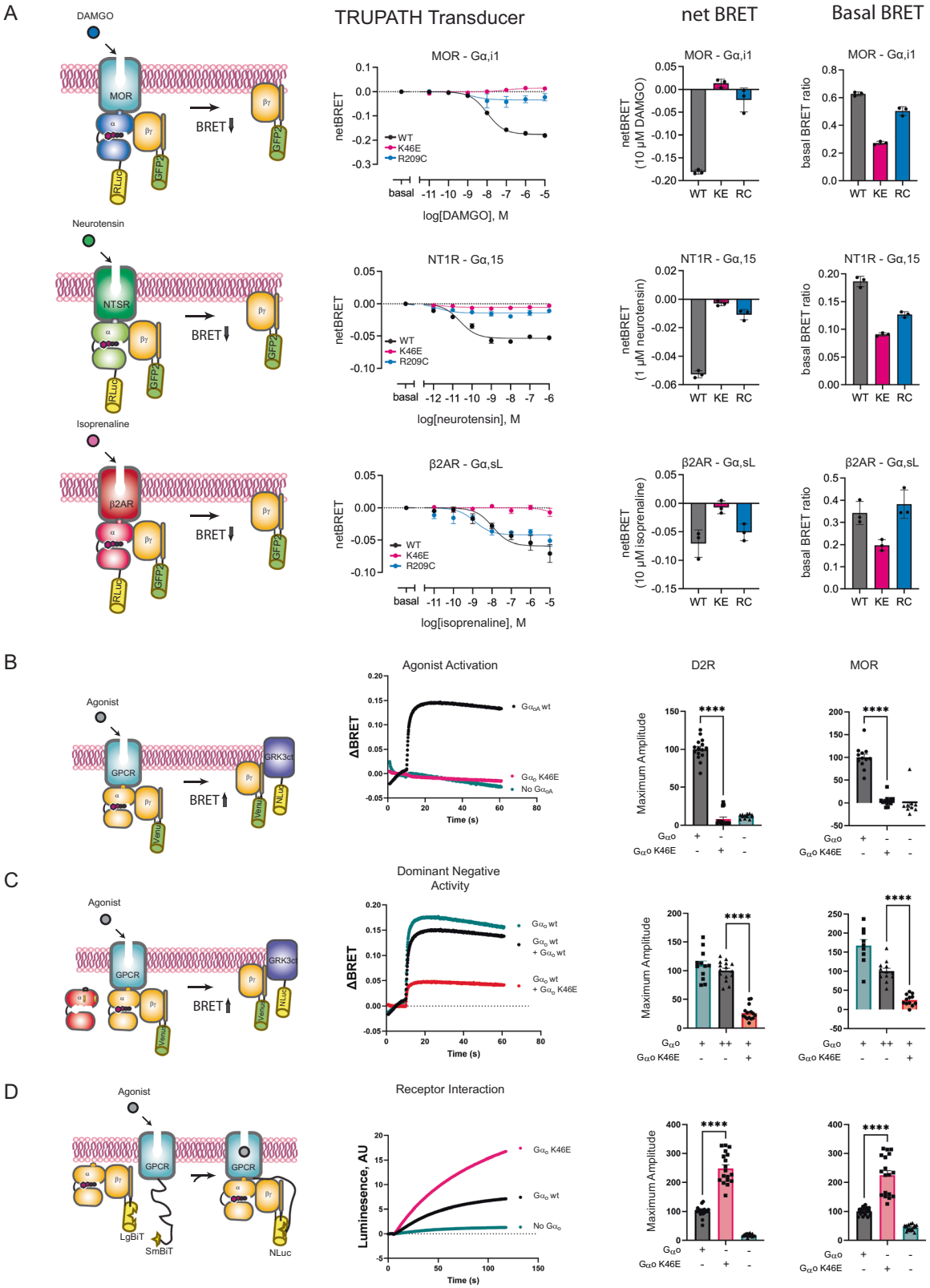

relies on complementation between SmBit-tagged receptor and LgBit-tagged Gβ. Assembly of receptor and Gβγ, and therefore of SmBit with LgBit, reconstitutes luciferase activity. In this case, binding of receptor to $G\alpha_o^{K46E}$ was higher by at least two-fold, in comparison with wild-type $G\alpha_o$ (Fig. 2D). This is in contrast to $G\alpha_o^{R209C}$, which binds to receptors in the manner of the wild-type G protein[24,27,32,33,37]. We conclude that both mutants sequester Gβγ, but pinKE alone sequesters receptors.

Inhibition of effector function

Our cell-based analysis revealed that $G\alpha_o^{K46E}$ inhibits receptor-mediated G protein activation and does so in a genetically dominant manner. Given that $G\alpha_o^{K46E}$ was identified in individuals with a severe neurological condition[38], and given that $G\alpha_o$ is the most abundant G protein in the brain and central nervous system[39,40], we next sought to establish its function towards a physiologically relevant effector

Fig. 2 | The pinKE mutation impedes G protein subunit dissociation. A Agonist-induced dissociation of Gα and Gβγ subunits (left). HEK293T cells transfected with the indicated receptor, WT or mutant Gα-RLuc8 donor, Gβ and Gγ-GFP acceptor proteins (middle). Representative concentration-response measurements using the μ-opioid (MOR; G_{i1}), neurotensin (NT1R; G_q, G_{13}), or β_2-adrenergic receptor (β_2AR; G_s) receptors, presented as fold decrease in dynamic range measured by comparing the energy transfer from donor to acceptor and reported as ΔBRET (GFP/Rluc8 per well minus Basal BRET, or GFP/Rluc8, at lowest dose of agonist) in comparison to basal activity, presented as raw BRET values prior to stimulus (right). Data are means ± SEM from 3 independent experiments, 2 measurements each. **B** Agonist-induced dissociation of Gβγ subunits (left). HEK293FT cells transfected with MOR or D2R, either empty vector (pcDNA3.1) or vector with wild-type or mutant $G\alpha_o$, masGRK3ct-Nluc-HA donor and Venus-Gβγ acceptor proteins. Representative time-course measurements for D2R after dopamine addition, presented as ΔBRET (ratio of emission by Venus at 535 nm and Nluc at 475 nm; recorded prior to agonist stimulation and subtracted from the experimental BRET values, middle). Effect of mutations, quantified as maximum amplitude relative to wild type (right). Data are means ± SEM from 4 (vector) or 5 ($G\alpha_o$ or $G\alpha_o^{K46E}$) independent experiments, 3 measurements each. **C** Dominant-negative inhibition of subunit release (left). HEK293 cells transfected as in **B** but with the addition of an equal amount of wild-type $G\alpha_o$ (middle), done by transfecting equivalent amounts of mutant and wild-type DNA. Effect of mutations quantified as maximum amplitude (right). BRET data are means ± SEM from 4 (vector) or 5 ($G\alpha_o$ or $G\alpha_o^{K46E}$) independent experiments, 3 measurements each. **D** Agonist-induced association of GPCRs and G proteins (left). HEK293FT cells transfected with MOR or D2R fused to myc-SmBiT, $G\alpha_o$, Gβ fused to LgBiT, and Gγ. Representative time-course measurements after dopamine addition leading to reconstitution of functional Nluc, presented as arbitrary luminescence units (ΔAU, middle). Effect of mutations, quantified as maximum amplitude (right). Data are means ± SEM from 6 independent experiments, 3 measurements each. Statistical analysis performed with 2-tailed unpaired *t* test; $^{****}p < 0.0001$. Source data are provided as a Source Data file.

system. We turned to the inwardly rectifying potassium (GIRK) channel, which like $G\alpha_o$ is abundant in the brain. Upon binding to free Gβγ, GIRK channel opening leads to potassium flux. The resulting current provides a readout of G protein heterotrimer dissociation (Fig. 3A).

To corroborate previous findings, we introduced to *Xenopus laevis* oocytes the GIRK1 and GIRK2 channels, followed by Gβγ and the $G\alpha_o$ protein variants (Fig. 3A). To establish the functionality of the GIRK channel, we measured the current in response to potassium, which provides a measure of basal (unstimulated) channel opening, and in response to barium, which inhibits channel current. Introduction of Gβγ alone activated the channel, and that activity was reduced by addition of $G\alpha_o^{R209C}$, presumably due to sequestration of Gβγ. In contrast, the signal was unaffected by the $G\alpha_o^{K46E}$ mutant and wild-type proteins (Fig. 3B, C). When we introduced the dopamine D_2 receptor and treated the cells with a saturating concentration of agonist (Fig. 3D), both mutants reduced the effect of potassium, and pinKE largely abrogated the effect of dopamine (Fig. 3E–G). These results are consistent with our initial screen[25], and support the model that the triadRC mutant sequesters Gβγ on its own while pinKE does so only in complex with the activated receptor.

To verify and expand our analysis, we used a human cell expression system (HEK293T) and measured activation of GIRK1/2 channels in cells co-expressed with either $G\alpha_o$, $G\alpha_o^{K46E}$ or $G\alpha_o^{R209C}$. We compared μ-opioid receptor activation with the direct activation of GIRK channels by alcohol (100 mM 1-propanol, PrOH). Alcohol-dependent activation bypasses G protein activation of GIRK channels[41,42], thus enabling a comparison between G protein-activated and directly-activated channels. The barium-inhibited current was not significantly different when comparing the wild type and mutant G proteins (Supplementary Fig. 1F), suggesting similar levels of GIRK expression. In contrast, we observed a significant reduction in the receptor-activated current, as compared to PrOH-activated current, with $G\alpha_o^{R209C}$ and an even stronger reduction with $G\alpha_o^{K46E}$ (Fig. 3H, I). Indeed, a large proportion (7/10) of recorded cells had PrOH-activated currents but negligible (<1 pA) responses to DAMGO, suggesting a dominant negative effect. These data support the conclusion that both $G\alpha_o^{K46E}$ and $G\alpha_o^{R209C}$ mutants sequester Gβγ, but $G\alpha_o^{K46E}$ does so only in the presence of activated receptor. Accordingly, differences in Fig. 3C, F could be due to stabilization by receptor of the G protein heterotrimer. Stated differently, triadRC acts as a Gβγ-specific dominant negative mutant and pinKE is a receptor-specific dominant negative mutant.

pinKE binds to Gβγ but not guanine nucleotides

Our cell-based measurements indicate that the pinKE variant can sequester receptors, possibly because it is locked in the nucleotide-free state. To test this directly, we purified $G\alpha_o^{K46E}$, as well as $G\alpha_o$ and $G\alpha_o^{R209C}$, and used three different measures of GTP binding and hydrolysis. First, we determined the melting temperature of purified protein using fast determination of quantitative cysteine reactivity (fQCR). In this method, buried cysteine residues that become exposed when the protein unfolds are covalently labeled with a fluorogenic compound. Previously we used fQCR to show that G proteins are more stable when bound to GTPγS than GDP[24,43], and we anticipated that the thermostability would be further reduced for a nucleotide-free mutant[44]. Accordingly, we purified wild type and mutant variants of $G\alpha_o$ and monitored labeling as a function of temperature. As shown in Fig. 4A, whereas the wild-type protein was more stable when bound to GTPγS than GDP, $G\alpha_o^{R209C}$ showed no stabilization in the presence of GTPγS. The $G\alpha_o^{K46E}$ variant had a substantially lower T_m, and likewise showed no differences when comparing GTPγS and GDP. Only at 1000-fold higher concentrations of GDP did we observe a T_m close to that of the wild-type protein (Fig. 4B).

Second, we tracked the ability of all three proteins to bind and hydrolyze GTP. To that end, we monitored the increase in fluorescence that accompanies the binding of BODIPY-GTP to protein, followed by the loss of fluorescence as BODIPY-GTP is reduced to BODIPY-GDP[45,46]. By this measure, we showed that the GTP analog bound to wild-type protein and $G\alpha_o^{R209C}$, but not to $G\alpha_o^{K46E}$ (Fig. 4C). GTP was slowly hydrolyzed by $G\alpha_o^{R209C}$, which is usually indicative of a hyperactive G protein. However, we have shown previously that substitutions of the triad-arginine suppress Gβγ dissociation, even in the GTP-bound state[24]. Thus, the slow rate of hydrolysis would not affect the levels of free Gα and Gβγ in the cell. Finally, to confirm that lack of binding was not an artifact of the BODIPY moiety, we measured the association of radiolabeled GTPγ^{35}S to the mutant and wild-type forms of $G\alpha_o$. Once again, nucleotide bound well to $G\alpha_o$ and $G\alpha_o^{R209C}$ but not to $G\alpha_o^{K46E}$ (Fig. 4D).

The lack of cooperativity in our thermostability profiles suggested that the pinKE mutant in the monomeric state is in a highly dynamic, and possibly molten, globular form. To determine whether $G\alpha_o^{K46E}$ was properly folded, we tested its ability to bind Gβγ directly, using bio-layer interferometry (BLI). We combined biotin-Gβγ, immobilized onto Streptavidin-coated biosensor tips, with a solution containing GDP and purified $G\alpha_o$, $G\alpha_o^{K46E}$, or $G\alpha_o^{R209C}$. After 10 min the tips were transferred to an identical solution but lacking Gα. By this measure, the wild type and mutant proteins exhibited similar association and dissociation kinetics, indicating that the binding affinities were the same for each (Fig. 4E). Taken together, our results indicate that both $G\alpha_o^{R209C}$ and $G\alpha_o^{K46E}$ stabilize the G protein heterotrimer but do so by different mechanisms. Whereas $G\alpha_o^{K46E}$ binds poorly to guanine nucleotides, $G\alpha_o^{R209C}$ binds to nucleotides but fails to release Gβγ.

To gain mechanistic insights into the residues that contribute to nucleotide binding affinity, we performed molecular dynamics simulations (MDS) on the monomeric form of wild-type $G\alpha_o$ and the two mutants, $G\alpha_o^{K46E}$ and $G\alpha_o^{R209C}$, with and without GTP bound. Using the aggregated trajectories from the MDS, we performed principal

https://doi.org/10.1038/s41467-024-50964-z

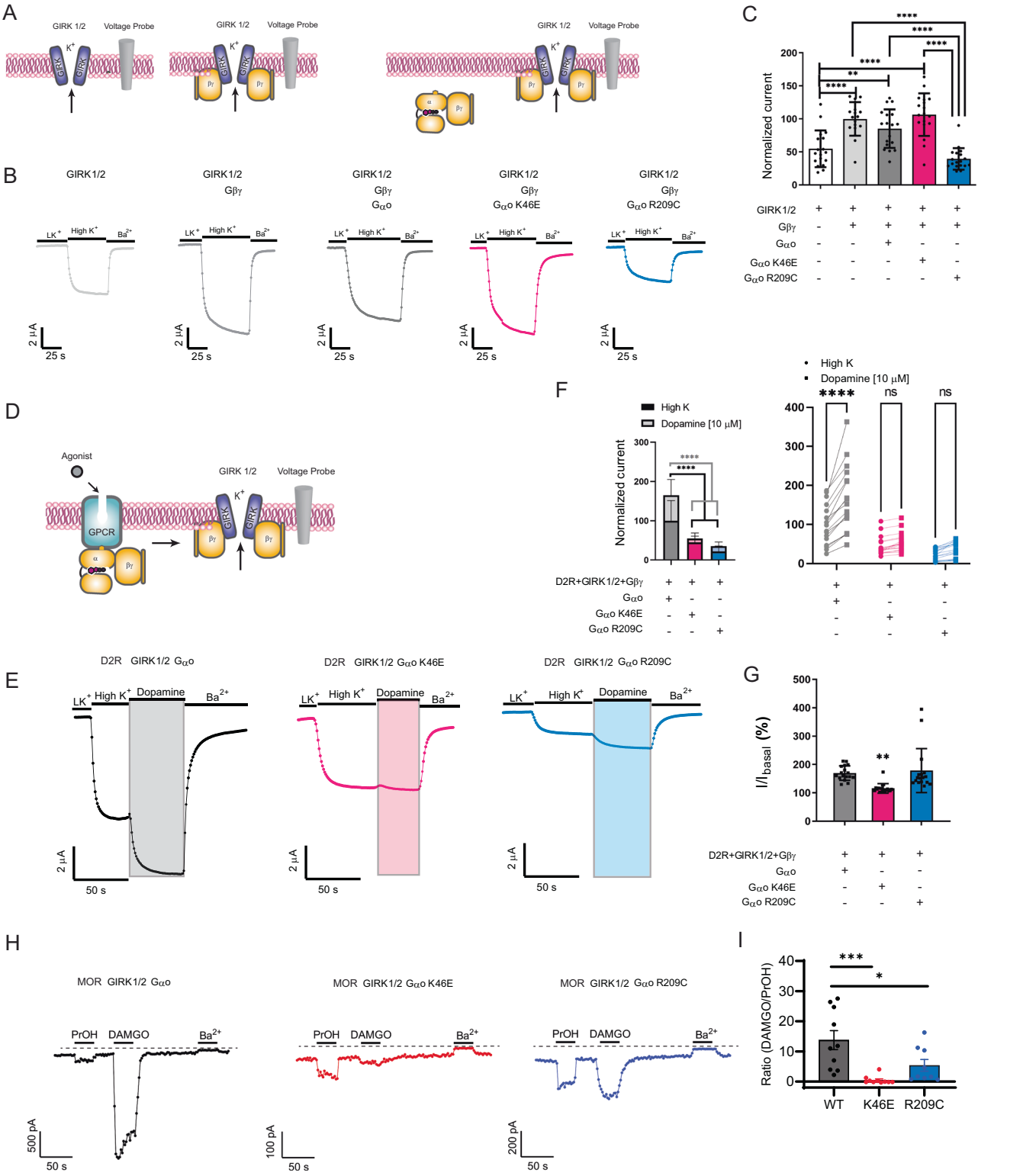

component analysis (PCA) and projected the free energy in the first two top-weighted principal components (PC1 and PC2). Figure 4F shows the free energy surface for monomeric $G\alpha_o$ and $G\alpha_o^{K46E}$, along with the structures representing the minima in the free energy surfaces. The $G\alpha_o^{K46E}$ mutant had fewer free energy minima, indicating less flexibility than that of the wild-type $G\alpha_o$. The structures representing the minima revealed that the Ras-like domain is more flexible in the mutant protein than it is in the wild type. To understand the residues in $G\alpha_o$ that contribute to GTP binding, we calculated the interaction energy (sum of electrostatic and van der Waals interaction energies) of GTP with the whole of $G\alpha_o$, $G\alpha_o^{K46E}$, or $G\alpha_o^{R209C}$. As seen in Fig. 4G, we observed significantly reduced interaction energy between GTP and the $G\alpha_o^{K46E}$ mutant, as compared to wild-type $G\alpha_o$ or $G\alpha_o^{R209C}$. We then examined the contact frequency (percentage of MD snapshots that make contact with GTP) of various residues in the nucleotide-binding site (Supplementary Fig. 2). This analysis revealed that residues Glu-43, Ser-44, Gly-45, Lys-46, Lys-181, and Thr-182 weaken their contact frequency by more than 30% in the $G\alpha_o^{K46E}$

Fig. 3 | The pinKE mutation impedes Gβγ-mediated effector activation. A GIRK1/GIRK2 channel current without (left) and with Gβγ (middle) or Gαβγ (right). **B** Representative two-electrode voltage clamp (TEVC) recordings in *Xenopus laevis* oocytes expressing GIRK1/2, $G\beta_1\gamma_2$, and either $G\alpha_o$ (black), $G\alpha_o^{K46E}$ (red) or $G\alpha_o^{R209C}$ (blue) following treatment with high potassium solution (High K^+) and barium (Ba^{2+}), which directly activate and inactivate the channel, respectively. **C** Maximum voltage differences. Normalized current, normalized to the GIRK 1/2 + Gβγ condition (100%). Data are means ± SD from 3 independent experiments with 6 measurements each; $^{****}p < 0.0001$; $^{**}p = 0.0083$. **D** GIRK1/GIRK2 channel current with Gαβγ and receptor. **E** Representative TEVC recordings in *Xenopus laevis* oocytes expressing dopamine D_2 receptor, GIRK1/2, $G\beta_1\gamma_2$, and either $G\alpha_o$ (black), $G\alpha_o^{K46E}$ (red), or $G\alpha_o^{R209C}$ (blue) following treatment with high potassium solution (High K^+) and barium (Ba^{2+}), as well as dopamine, which activates the D_2 receptor. **F** Normalized potassium- and dopamine-induced currents. Data are means ± SD from 3 independent experiments, with 6, 6, and 5 measurements each; $^{****}p < 0.0001$. **G** Normalized currents induced by dopamine divided by currents induced by high potassium (I/Ibasal). Data from (**F**) are means ± SD; $^{**}p = 0.0039$. **H** Representative current recordings from HEK293T cells expressing MOR and the indicated $G\alpha_o$ subunit, showing activation with 1-propanol (PrOH), activation with DAMGO or inhibition with $BaCl_2$. Each solution was delivered for 30 s. **I** Bar plot shows the ratio of DAMGO-activated to PrOH-activated current for each $G\alpha_o$ subunit. Data are means ± SD from 9 (R209C) or 10 (WT, K46E) independent experiments; $^{***}p = 0.0003$; $^{*}p = 0.0221$. Statistical analysis in **C** and **G** performed with one-way ANOVA Tukey's test. Statistical analysis in **F** performed by two-way ANOVA with Tukey's multiple comparison (left) and Sidak pairwise comparison (right) tests. Statistical analysis in **I** performed with one-way ANOVA Dunett's test. Source data are provided as a Source Data file.

mutant as compared to wild-type $G\alpha_o$. The total interaction energy of the α5 helix with the Ras domain is weaker in $G\alpha_o^{K46E}$ than in wild-type $G\alpha_o$; similarly, the structure of the previously described GDP-bound $G\alpha_o$–^{4A} mutant shows that the α5 helix is detached from the Ras domain[18]. These data suggest that the K46E and −4A mutants operate by similar mechanisms. In summary, our MDS analysis reveals how the Lys-46-Glu substitution affects the structure and dynamics of $G\alpha_o$, and provides a rationale for the observed reduction in GTP-binding affinity.

pinKE preserves a high-affinity agonist-bound form of the receptor

Agonist binding to receptor stabilizes the nucleotide-free form of the G protein and, conversely, the nucleotide-free G protein confers increased affinity of receptors for agonists (but not for antagonists)[47]. Because pinKE binds poorly to nucleotide, we anticipated that it would lock the receptor in the activated, agonist-bound conformation. We initially tested this using a saturation binding assay to determine affinity for radioactive agonist, comparing $G\alpha_o$ and $G\alpha_o^{K46E}$ in the presence and absence of the GTP analog GppCp. To ensure proper coupling and a 1:1 stoichiometry, we used a fusion of the μ-opioid receptor and $G\alpha_o$ (MOR-$G\alpha_o$). As anticipated by our model, MOR-$G\alpha_o^{K46E}$ bound agonist with high affinity, even in the presence of GppCp; in contrast, MOR-$G\alpha_o$ displayed decreased affinity for agonist with addition of GppCp (Fig. 5A–C, black vs red traces). Furthermore, we purified the full-length dopamine D_2 receptor gene (without any mutations, D2R) co-expressed in sf9 insect cells with $G\alpha_o^{K46E}$, $G\beta_1$, and $G\gamma_2$, in the presence and absence of apyrase, an enzyme that degrades ATP/GTP to AMP/GMP, using the full agonist dopamine to form the complex. Size exclusion and SDS gel analysis revealed that complex formation is achieved and stable during cell lysis throughout the multi-day purification process, even in the absence of apyrase (Supplementary Fig. 3). Taken together, these results indicate that $G\alpha_o^{K46E}$ imposes the high affinity agonist-binding conformation of the receptor, and does so even in the presence of guanine nucleotide.

Our results indicate that a single amino acid substitution confers stable association of $G\alpha_o$ with agonist-bound receptor and the Gβγ subunits. Accordingly, the pinKE mutant could be used for structure determination of receptors bound to G proteins. To test this, we solved the structure of the mutant complex using cryo-EM. For these studies we used the full-length dopamine D_2 receptor (D2R) coexpressed with $G\alpha_o^{K46E}$, $G\beta_1$, and $G\gamma_2$, in the presence and absence of the $G_{i/o}$ protein-stabilizing single chain antibody scFv16[48]. scFv16 binds to the N-terminus of the α subunit and is used in structural studies to prevent dissociation of the G protein ternary complex[48]. The full agonist dopamine was used to form the ligand-bound receptor-G protein complexes. We determined the structures of the dopamine-bound D2R-$G\alpha_o^{K46E}$ complex, with and without scFv16, with overall resolutions of 3.3 Å and 3.2 Å, respectively (Fig. 5D, E; Supplementary Figs. 4 and 5; and Supplementary Table 1).

The two structures (D2R-G_o^{K46E} +/− scFv16) were readily superimposable and with only discreet differences, having a root mean square difference (RMSD) of 0.69 Å for all aligned Cα's. The EM density was well resolved for the Ras-like domain along with the C-terminal α helix of each G protein complex. However, the EM density for the all-helical domain (AHD) in the scFv16 structure was much weaker in intensity and less resolved when compared to the structure in the absence of scFv16, at the same EM density contour level, and was not modeled into the structure. It is important to note that the scFv16 in our complex did not appear to clash with the AHD and did not prevent complex formation (scFv16 was co-expressed with receptor and G protein subunits). In the D2R-G_o^{K46E} (- scFv16) structure, Gα was in the open conformation with the AHD interacting with the outermost β strand of the WD3 repeat of the $G\beta_1$ subunit. The position of the AHD in our structure is most similar to that seen in the NTR1 neurotensin receptor and G_{i1} protein complex (PDB ID: 7L0Q)[49], in which the αA helix of the AHD is almost perpendicular with the $G\beta_1$ subunit (~80° angle relative to the Gα αN helix). In contrast, in the β_2-adrenergic receptor-G_s protein complex crystal structure (PDB ID: 3SN6)[17], the AHD is positioned further from the Ras-like domain, possibly due to the presence of a stabilizing nanobody at the domain interface or due to crystal packing or both; the AHD αA helix is parallel with the G_s N-terminus (~0° angle relative to the Gα αN helix) and has no apparent interaction with the WD3 repeat of the $G\beta_1$ subunit (Supplementary Fig. 6).

In the high-resolution crystal structures of the heterotrimeric G_{i1} protein complex (PDB ID: 1GP2) bound to GDP[50] and the $G\alpha_{i1}$ subunit bound to GTP (PDB ID: 1GIA), the conserved Lys-46 is engaged in a charged interaction with the β phosphate group of the bound GDP/GTP. Additionally, the $G\alpha_{i1}$ lysine is engaged in charged interactions with the Ser-44 hydroxyl and the backbone carbonyl of residues Gly-40 and Ala-41 of the loop region between sheet β1 and helix α1, essentially creating a positively charged pocket in which the GDP phosphate groups reside (Fig. 1). Conversely, in our D2R-G_o^{K46E} structure, there is no bound nucleotide while the Glu-46 is engaged in weak charged interactions with backbone carbonyl and backbone amide of Gly-40 through Gly-45 loop residues. Superposition with the same region in the $G\alpha_{i1}$ structure, along with electrostatic analysis, revealed that the K46E substitution causes a slight rearrangement of the aforementioned loop (RMSD of 1.094 Å and 0.598 Å when comparing $G\alpha_{i1}$-GTP (PDB ID: 1GIA) with D2R-G_o^{K46E} and D2R-G_o^{K46E} + scFv16, respectively) and is shifted toward the front of the pocket along with a charge reversal to a negatively charged pocket (Fig. 5D, E). Thus, the pinKE mutant occludes and electrostatically repels GDP, providing a structural explanation for the properties of the mutant with respect to nucleotide affinity and structural stability.

To date, there exist three active state structures of D2R in complex with a G protein (PDB ID: 6VMS, 7JVR, and 8IRS). However, these structures are in complex with G_{i1}, not G_o, and bound with the agonists rotigotine or bromocriptine, not dopamine. Superposition

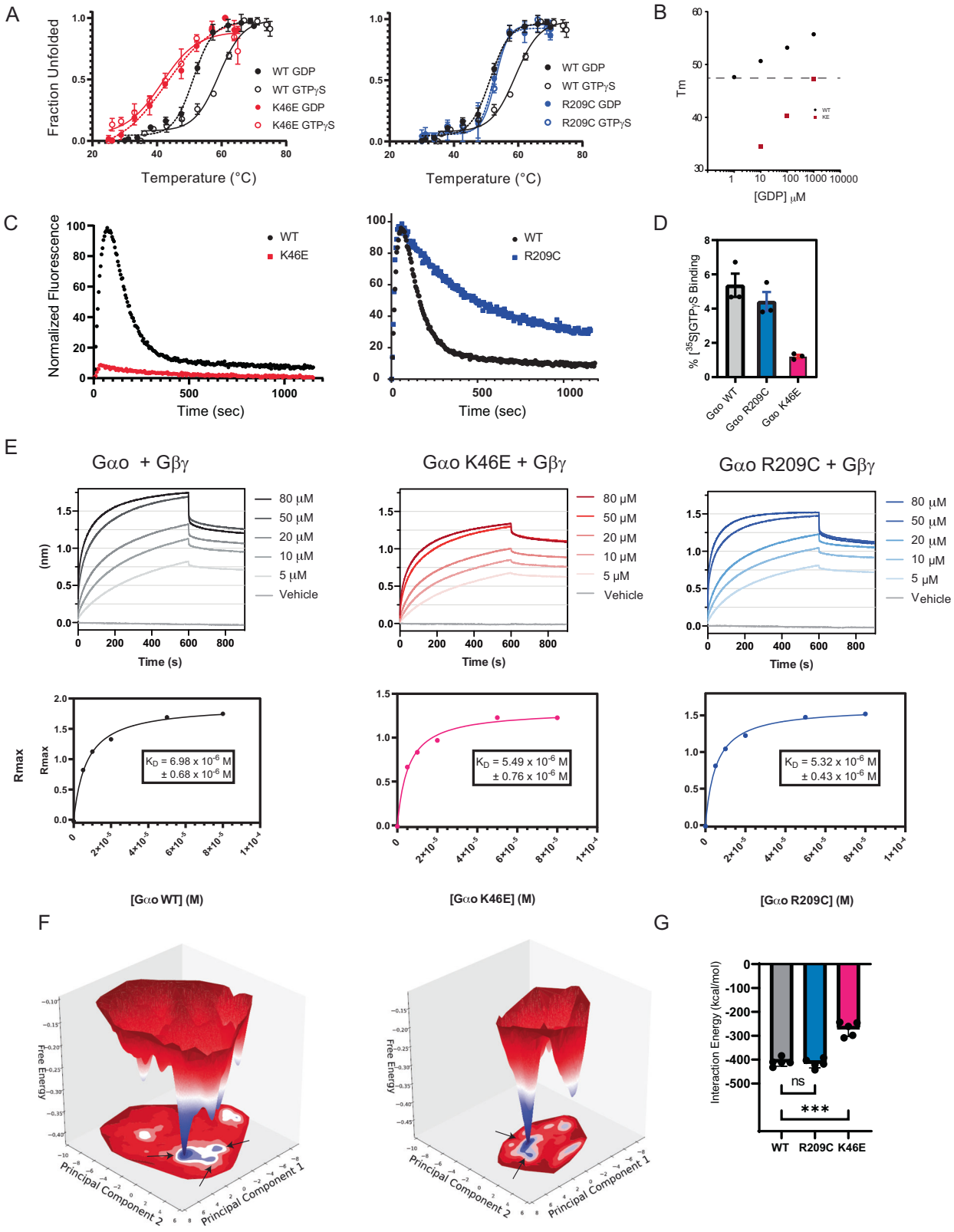

of the receptors from our D2R-G_o^{K46E} structure (without scFv16) and from D2R-G_{i1} (PDB ID: 8IRS) reveals an RMSD of 1.50 Å of all aligned α carbons (Fig. 6A). Most of the divergence between the two structures is at the extracellular ends of the transmembrane (TM) domains and in the extracellular loops. In comparison to D2R-G_{i1}, TM5 and TM6 in the D2R-G_o^{K46E} structure are more ordered, have more α helical content and are extended by 3 and 5 residues, respectively. In contrast, the orthosteric binding site residues superpose well in the two structures. The bound ligands occupy a similar area and engage overlapping residues, even though rotigotine is larger than dopamine and thus occupies more buried surface area (bsa) (272 $Å^2$ versus 131 $Å^2$, Fig. 6B and Supplementary Table 2). Furthermore, a comparison of our dopamine-bound D2R complex with the dopamine-bound D1R structure (PDB ID: 7F1O) revealed

https://doi.org/10.1038/s41467-024-50964-z

Fig. 4 | The pinKE mutation preserves high affinity binding to Gβγ but not guanine nucleotides. A Thermostability of purified $G\alpha_o$ (black), $G\alpha_o^{K46E}$ (red), and $G\alpha_o^{R209C}$ (blue) equilibrated in GTPγS (solid lines) or GDP (dashed lines). T_m values were quantified by fitting a two-state model of thermal unfolding. **B** Comparison $G\alpha_o$ and $G\alpha_o^{K46E}$ binding (T_m) to GDP. **C** Combination of purified $G\alpha_o$, $G\alpha_o^{K46E}$, and $G\alpha_o^{R209C}$ with BODIPY-GTP to monitor binding (increase in fluorescence) and hydrolysis (decrease in fluorescence). Normalized fluorescence, defined as percentage of maximum signal after subtracting the starting signal, for each experimental run. **D** Percent $G\alpha_o$ bound to GTPγ[^{35}S] determined using the ratio of the measured activity per sample (cpm/pmol $G\alpha_o$) to the average total specific activity of ^{35}S added to each sample (cpm/pmol). **E** Purified biotinylated Gβ and Gγ immobilized on streptavidin were combined with the indicated concentration of purified $G\alpha_o$ (left), $G\alpha_o^{K46E}$ (middle), and $G\alpha_o^{R209C}$ (right). Binding is reported as a shift in the interference pattern (nanometers, nm). Rmax, defined as the absolute signal in nm after subtracting the starting (buffer) control. **F** Free energy surface of $G\alpha_o$-apo system (left) and $G\alpha_o^{K46E}$ -apo system (right). Shown are representative structures from the local minima indicated by arrows on the free energy surface. **G** Interaction energy of GTP with proteins in the $G\alpha_o$-GTP, $G\alpha_o^{R209C}$-GTP, and $G\alpha_o^{K46E}$ -GTP systems. Data in **A** and **D** are means ± SEM, from 3 independent experiments, 3 measurements each. Data in **B** are means of 2 independent experiments. Data in **C** are representative of 3 or more independent experiments. Data in **E** are representative of 2 independent experiments, 2 measurements each. Data in **G** are means ± SEM, from 5 independent experiments; $^{***}p = 0.0003$. Source data are provided as a Source Data file.

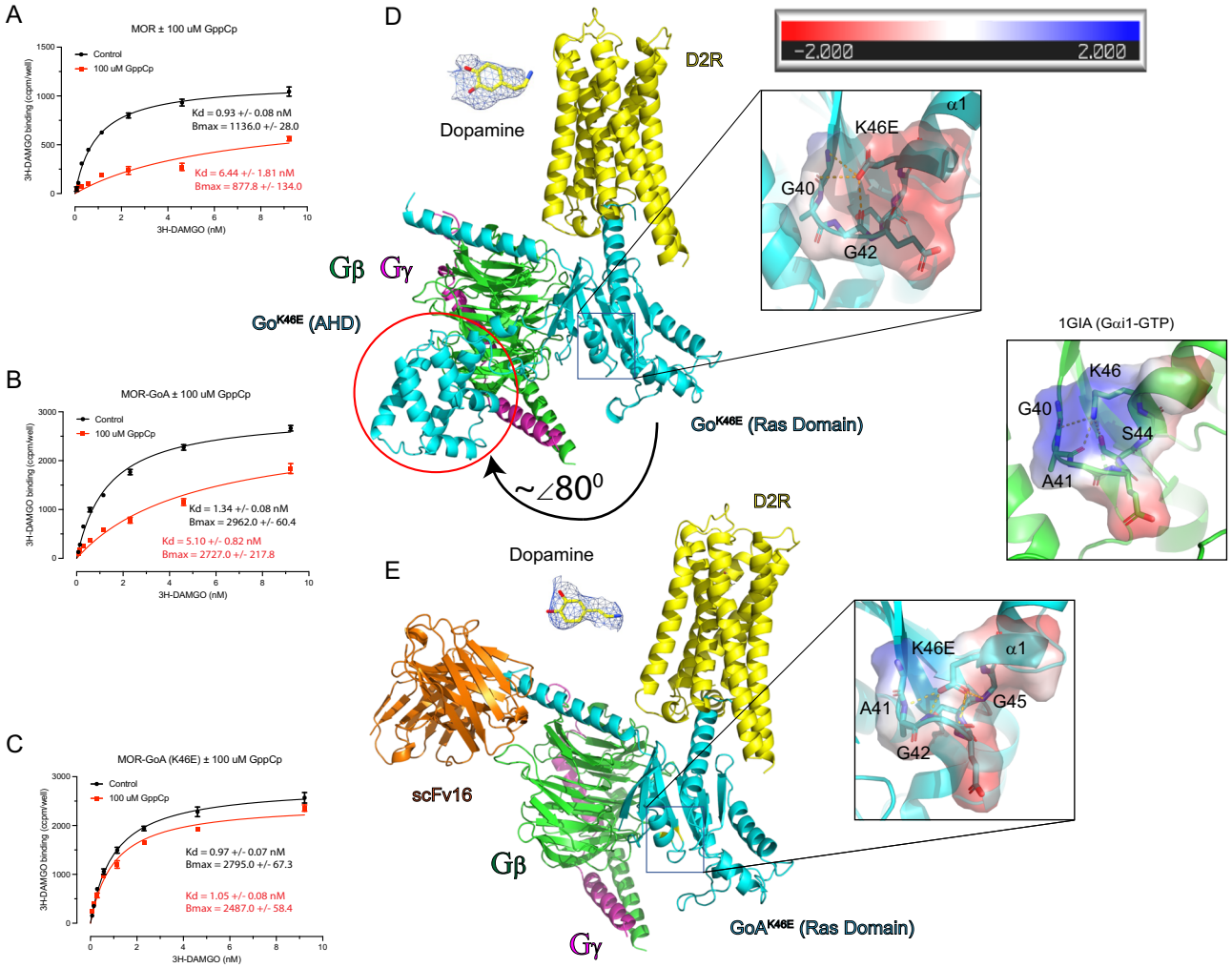

Fig. 5 | The pinKE mutation stabilizes the high affinity agonist-bound form of the receptor. A Saturation binding assays using [^{3}H] DAMGO in the absence (black) and presence (red curve) of nonhydrolyzable GTP (GppCp) for μ-opioid receptor (MOR), 15 μg/well. **B** As in **A**, but for MOR fusion with $G\alpha_o$, 15 μg/well. **C** As in **A**, but for MOR fusion with $G\alpha_o^{K46E}$,12 μg/well. **D** Cryo-EM structure of the dopamine D_2 receptor (D2R), $G\alpha_o^{K46E}$ and Gβγ complex. Insets show representative EM density for dopamine and the K46E region of $G\alpha_o$ (note occluded pocket and charge reversal). Distance lines are <4 Å. Black directional arrow, movement of the all-helical domain (AHD, enclosed by a red circle) away from Ras-like domain. Inset, electrostatic potential calculated using the APBS plugin for PyMol. Displayed is the colored surface with a range of ±2 K_bT/e_c. **E** Cryo-EM structure of D2R, $G\alpha_o^{K46E}$, Gβγ, and scFv16 complex. Insets show representative EM density for dopamine and the Lys-46 region in $G\alpha_{i1}$ (PDB ID: 1GIA, note positive charge of region). Distance lines are <4 Å. Inset, electrostatic potential calculated using the APBS plugin for PyMol. Displayed is the colored surface with a range of ±2 K_bT/e_c. Data in **A**–**C** are presented as means ± SEM from independent experiments, 3 measurements each. Statistical differences of K_d values derived from concentration-response assays were determined using the Extra sum-of-squares F test function in GraphPad Prism 9.0 comparing ±100 μM GppCp: (**A**) $p < 0.0001$; $F(1,185) = 35.5$ (**B**), $p < 0.0001$; $F(1,188) = 62.2$; (**C**) $p = 0.5185$; $F(1,186) = 0.4185$. In panels **D** and **E**, superposition of loop region residues G40-S47 Cα reveal an RMSD of 1.094 Å and 0.598 Å when comparing $G\alpha_{i1}$-GTP (PDB ID: 1GIA) with D2R-G_o^{K46E} and D2R-G_o^{K46E} + scFv16, respectively. Source data are provided as a Source Data file.

https://doi.org/10.1038/s41467-024-50964-z

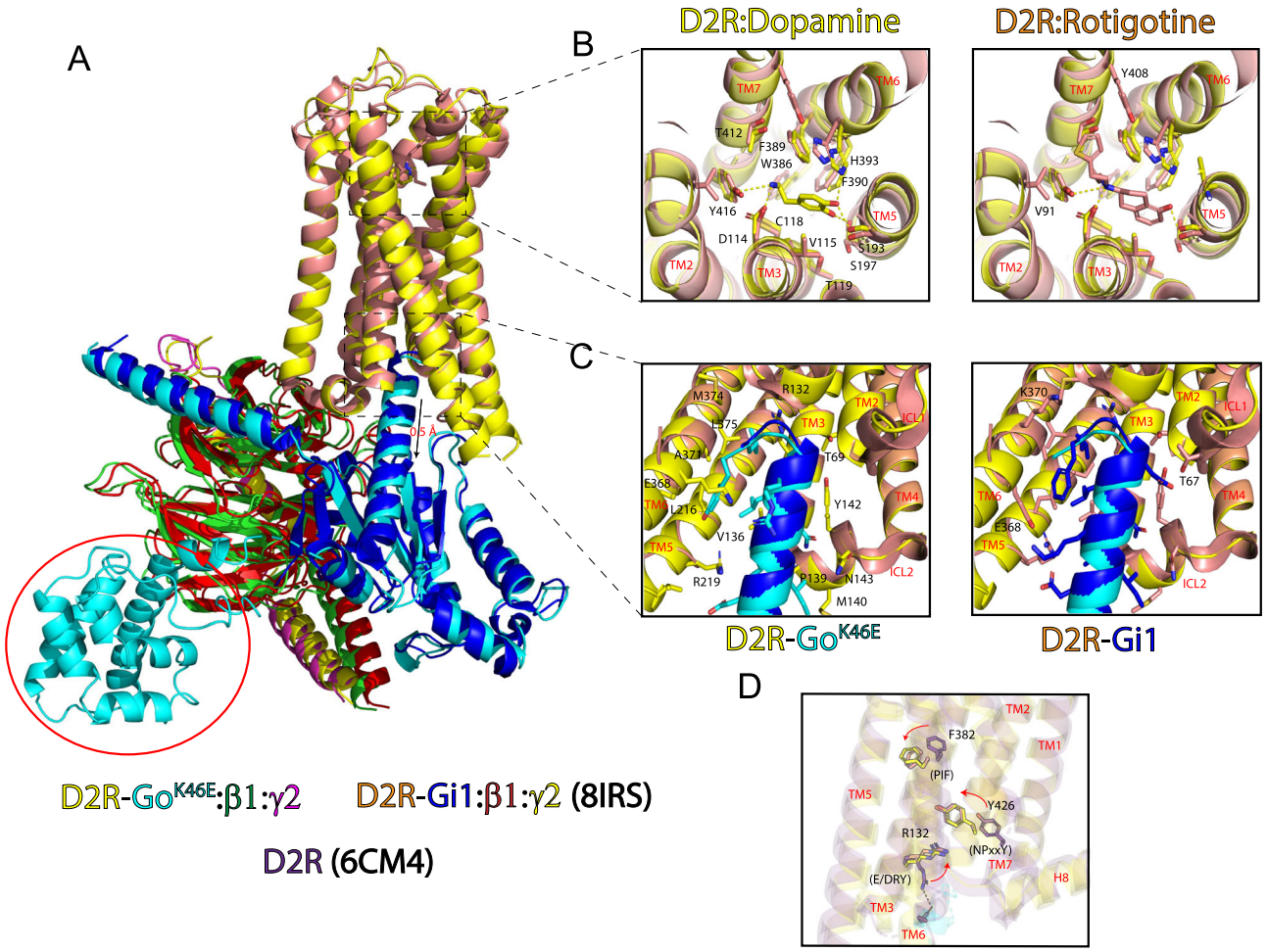

Fig. 6 | Structural comparison of D2R-G_o^{K46E} with D2R-G_{i1} reveals conserved features. A Superposition of D2R-G_o^{K46E} bound with dopamine and D2R-G_{i1} bound with rotigotine (PDB ID: 8IRS) reveals an RMSD of 1.50 Å between the two receptors. $G\alpha_o^{K46E}$ is shifted downward approximately 0.5 Å relative to $G\alpha_o$. **B** Top-down view of the extracellular region and orthosteric binding sites of D2R-G_o^{K46E} and D2R-G_{i1}. Stick figures are residues that interact with either dopamine or rotigotine. Yellow distance lines are <4 Å. Stick figures of residues and bound ligand correspond to the receptor complex. Left panel, stick figures are shared residues; right panel, residues specific for rotigotine. TMs are labeled in red. **C** Comparison of intracellular region of D2R-G_o^{K46E} and D2R-G_{i1}. Stick figures are interacting residues from D2R and the respective G protein C-terminal tails. Stick figures of residues correspond to the receptor complex. Left panel, stick figures of shared residues; right panel, additional residues specific for G_{i1}. TMs and intracellular loops (ICLs) are labeled in red. **D** Structural comparison of GPCR activation motifs in the D2R inactivate state (PDB ID: 6CM4) and those of D2R-G_o^{K46E} and D2R-G_{i1}. Stick figures, key residues in the PIF, E/DRY, and NPxxY activation motifs. Arrows, direction of movement in going from the inactive to the active state. Coloring is consistent with the corresponding D2R.

that the binding-site residues are conserved in these receptor subtypes (Supplementary Table 2).

Comparison of the intracellular interface of D2R-G_o^{K46E} and D2R-G_{i1} revealed an approximate 0.5 Å off-center shift of the two G protein heterotrimer complexes, a difference that reverberates through the complex (Fig. 6A). For the D2R-G_o^{K46E} complex, $G\alpha_o$ contributes 12 sidechain residues and 915 Å^2 of bsa to the interface; the C-terminal α-helix alone contributes 9 out of 12 residues and 773 Å^2 of the total bsa (Supplementary Table 3). For the D2R-G_{i1} complex, $G\alpha_{i1}$ contributes 16 sidechain residues and 940 Å^2 of bsa to the interface; the C-terminal α-helix contributes 12 out of 16 residues and 808 Å^2 of the total bsa (Supplementary Table 4). Conversely, the D2R receptor contributes 16 and 19 sidechain residues to the G_o and G_{i1} protein interfaces, respectively, 14 of which are shared between the two structures (Fig. 6C).

Activation motif changes in GPCRs signify a transition from the inactive to active state, and vice versa. Rearrangement of the phenylalanine in the PIF connector region, rotation of the tyrosine in the tyrosine toggle switch (NPxxY), and disruption of an ionic-lock in the E/DRY motif have all been reported to be important for receptor activation, but can be receptor- and ligand-specific[51]. The PIF connector motif is likely to have an important role in connecting the agonist binding pocket to downstream conformational rearrangements required for receptor activation[17]. The NPxxY and E/DRY motifs have been proposed as stabilizing elements of an active conformation[52,53]. These motifs are superimposed in the activated D2R-G_o^{K46E} and D2R-G_{i1} structures, and far less so when compared to the inactive D2R receptor structure (PDB ID: 6CM4)[54] (Fig. 6D). Thus, structurally speaking, the single substitution in G_{oA}^{K46E} has no apparent negative impact on ligand binding or activation of D2R. We conclude that the pinKE mutation locks the receptor in the agonist-bound, transitory pre-activated state.

Discussion

G proteins are among the most studied of all enzymes. Detailed biochemical and structural analyses have revealed the molecular transitions leading to subunit dissociation and the conversion of GTP to GDP. In contrast, little is known about the molecular properties of the

apo form of the protein, which is needed to exchange GDP for GTP. In cells, it exists only transiently, during activation by agonist-occupied receptors. In vitro, it is unstable and has proven difficult to isolate and characterize biochemically[55]. Here we describe a Gα variant that favors the nucleotide-free conformation of the protein yet binds with normal affinity to Gβγ and remains in a non-productive complex with receptor. Thus, pinKE sustains the first committed step of G protein activation.

Looking forward, we expect that pinKE will help to accelerate structure determination of G protein ternary complexes. Prior efforts have relied on the simultaneous assembly of agonist, receptor, and G protein heterotrimer, with removal of guanine nucleotides using the enzyme apyrase. This approach was used to solve the first crystal structure of a receptor-G protein complex, a breakthrough that provided details about conformational changes in Gα during nucleotide release[17], and that provided important mechanistic details of a critical, but ephemeral, step of the G protein activation cycle. Indeed, these rearrangements are by far the most dramatic of the various conformational changes in the G protein, including those leading to subunit dissociation or engagement with effectors and RGS proteins. Subsequent studies used variants of Gα containing 4-8 mutations (none of which target the pinK or triadR)[56,57], shown previously to destabilize nucleotide binding[58,59]. The structure of the all-helical domain was not well resolved in those efforts. In comparison, we have determined the structure of the receptor and G protein heterotrimer, including much of the all-helical domain, using a single well-characterized substitution in Gα.

The pinKE allele may also prove useful for high-throughput drug screening programs. Just as agonist binding stabilizes the apo form of the G protein, the apo form of the G protein confers increased affinity of receptors for agonists (but not for antagonists). By directly comparing binding of ligands in cells that express pinKE with those that express wild-type G protein, it should be possible to rapidly differentiate agonists from antagonists, since only agonists will bind preferentially to receptors in cells expressing the mutant allele. Any drug screening programs may be carried out experimentally as well as computationally, in conjunction with molecular docking programs and with virtual chemical libraries[60].

In this work, we establish a potential mechanistic basis for human disease. The $G\alpha_o{}^{K46E}$ and $G\alpha_o{}^{R209C}$ mutations have been implicated in a pathogenic condition characterized by seizures, movement disorders, intellectual disability, and developmental delay[37,40,61–64]. One individual with the K46E mutation exhibited focal, tonic, spasm, and tonic spasm seizures beginning 6 h after birth[38]. That individual died in her sleep at 23 months of age. Individuals with the R209C mutation are far less likely to have seizures but do exhibit involuntary movement, difficulty speaking, as well as intellectual and developmental delay[65,66]. In our analysis, both mutations lead to sustained assembly of $G\alpha_o$ with Gβγ, and in both cases result in diminished activation of effector channels. However, our analysis reveals that these two mutants have distinct molecular properties; whereas the pinKE mutant binds poorly to nucleotide and, consequently, forms a non-productive complex with receptors and Gβγ, the triadRC mutant binds strongly to the Gβγ subunits, regardless of bound nucleotide[24]. Given that both residues are conserved in all G proteins, the mechanisms detailed here are likely to be universal for all subtypes and species. More broadly, our mechanistic analyses of $G\alpha_o$ variants illustrate how small changes at the molecular level (e.g. a single amino acid substitution) can lead to broader consequences at the cellular and organismal level. Such insights may eventually reveal potential treatments for the associated neurological disorders in humans. Just as a detailed understanding of the molecular basis for ligand binding has led to important advances in receptor pharmacology, a better understanding of nucleotide exchange mechanisms could reveal strategies to compensate for the genetic defects that cause disease. Potential treatments might include ligands that bind to and regulate GPCRs[23], G proteins[67–71], and G protein-regulated potassium channels[72]. However, and most importantly, the mechanistic differences between the pinKE and triadRC mutants indicate that different treatment strategies will likely be needed to treat what has long been considered a single disease entity.

Methods

Mutagenesis and plasmid construction

Primestar Max (Takara Bio; R045A) mutagenesis was performed using primer pairs, each containing 5 bp 5′ and 20-30 bp 3′ to the relevant codon, and are provided in Supplementary Table 5.

Complete sequences for parent plasmids generated in this study are provided in Supplementary Information: PET-SUMO-$G\alpha_o$ for purification, pMAX-$G\alpha_o$ for GIRK assays in *X. oocyes*, pcDNA3.1-$G\alpha_o$ for GIRK assays in HEK293 cells, MOR-$G\alpha_o$ fusion for radioligand binding, and pFastbac-$G\alpha_o$ for cryo-electron microscopy.

Bioluminescence resonance energy transfer

Basal association and receptor-mediated dissociation of Gα and Gβγ were determined by BRET[31]. HEK293T cells (ATCC; CRL-11268) were maintained at 37 °C in Dulbecco's Modified Eagle Medium (DMEM) (Corning; 10-017-CV) supplemented with 10% FBS (GIBCO; A3382001), 100 I.U./mL penicillin, and 100 mg/mL streptomycin. Cells were then co-transfected with a 1:1:1:1 ratio of plasmids containing the human receptor, Gα (multiple isoforms, wild-type and mutant constructs) fused to *Renilla* luciferase 8 (Rluc8), Gγ (multiple isoforms) fused to GFP2 and Gβ (multiple isoforms) using TransIT-2020 (Mirus) transfection reagent following manufacturer guidelines. The next day, cells were plated into poly-L-lysine coated 96-well white clear bottom plates (Greiner Bio-One; 655098) at a density of ~60,000 cells/well in DMEM supplemented with 1% dialyzed FBS, 100 I.U./mL penicillin, and 100 mg/mL streptomycin. The following day, cells were washed with assay buffer (Hank's Balanced Salt Solution containing 20 mM (4-(2-hydroxyethyl)−1-piperazineethanesulfonic acid) (HEPES), 0.1% bovine serum albumin, and 0.01% ascorbic acid, pH 7.4,), then incubated with 60 µL assay buffer containing 7.5 µM coelentrazine 400a (Nanolight; 340). After 10 min in the dark, 30 µL (3X concentration) of agonist in drug buffer was added to each well. After another 10 min in the dark the plates were serially read five times using a PheraSTAR FSX plate reader with 395 nm (Rluc8-coelenterazine 400a) and 510 nm (GFP2) filters for 1 sec per well. Measurements from the final read were used for all analyses. The BRET ratio was calculated as the ratio between acceptor (GFP) and donor (Rluc8) emission values. ΔBRET values were determined by subtracting the BRET ratio from cells treated with vehicle from the entire dataset. ΔBRET data for each dose-response curve were fit using the log(inhibitor) vs. response (three parameter) function in GraphPad Prism (GraphPad Software Inc., San Diego, CA) with the top fit parameter constrained to 0. Expression of Gα was verified by western blotting.

Basal and receptor-mediated association of $G\beta_1\gamma_2$ and masGRK3ct was determined by BRET[36]. HEK293FT cells (Thermo Fisher Scientific; R70007) were grown at 37 °C in Dulbecco's modified Eagle's medium (Thermo Fisher Scientific;11965-092) + 10% fetal bovine serum (Millipore Sigma; 12303 C), minimum Eagle's medium non-essential amino acids (Thermo Fisher Scientific;11140-050), 1 mM sodium pyruvate[34,36]. Approximately 50,000 cells per well were distributed in 96-well flat-bottom white microplates (Greiner Bio-One; 655073) and transfected with plasmids encoding the human Flag-tagged dopamine D_2 receptor (DRD2)[73] or human µ-opioid receptor (OPRM1)[74], as well as masGRK3ct-Nluc (comprised of the C-terminal 141 amino acids of GRK3, an N-terminal peptide directing myristoylation, the HA epitope tag and Nano luciferase)[36], human $G\gamma_2$ fused to residues 1-155 Venus (Venus 1-155-$G\gamma_2$)[34], human $G\beta_1$ fused to Venus 156-239 (Venus 156-239-$G\beta_1$)[34], and human $G\alpha_o$ or $G\alpha_o{}^{K46E}$ (constructs described above) in a 1:1:1:1:2 ratio, carried out using Lipofectamine LTX Reagent with PLUS (Thermo Fisher Scientific; 15338100). After 16-24 hr the cells were

washed once with BRET buffer (Dulbecco's Phosphate-Buffered Saline (PBS) + 0.5 mM $MgCl_2$ and 0.1% glucose) and resuspended in 50 mL BRET buffer. Fifty µL of the Nluc substrate furimazine (Promega; N1120) in BRET buffer was added per well, as directed by the manufacturer, followed by 50 µL (3X concentration) of 100 µM dopamine (Millipore Sigma; H8502) or 10 µM DAMGO (Adipogen; AG-CP3-0005V-M001). The plates were read using a PHERAstar FSX microplate reader (BMG Labtech) equipped with two emission photomultiplier tubes, allowing detection of two emissions simultaneously with a highest possible resolution of 20 ms per data point. All measurements were performed at 37°C. The BRET signal was determined by calculating the ratio of the light emitted by the Venus-G$\beta_1\gamma_2$ (535 nm ± 30 nm) over the light emitted by the masGRK3ct-Nluc-HA (475 nm ± 30 nm). The average baseline value (basal BRET ratio, with no Gα transfected) recorded prior to agonist stimulation was subtracted from the experimental BRET signal values.

Basal association and receptor-mediated dissociation of receptors and G$\beta_1\gamma_2$ was determined using the NanoBiT assay[37]. Briefly, 4,000,000 HEK293FT cells in 60 mm dishes transfected with plasmids encoding either the human dopamine D_2 receptor (D2R)[37] or human µ-opioid receptor (MOR)[74], each fused to the myc epitope tag and SmBiT, as well as human Gβ_1 fused to LgBiT[37] and human Gγ_2 (cDNA Resource Center; GNG0200000). Transfected cells were harvested, washed in PBS, 5 mM EDTA, collected by centrifugation at 500 x*g* for 5 min resuspended in BRET buffer and distributed in 96-well plates as explained above. Furimazine (Promega; N1120, 750x diluted Nano-Glo substrate) in BRET buffer was added to transfected cells in 96-well plates and after 1 min to stabilize the brightness of luminescence before addition of dopamine or DAMGO. Luminescence was measured using a PHERAstar FSX plate reader at 37 °C.

No commonly misidentified cell lines were used in the study. HEK293 cell lines were from commercial sources and not independently authenticated. All cell lines tested negative for mycoplasma contamination.

GIRK channel activity measurements

Two-electrode voltage clamp (TEVC) methods. Complementary DNA constructs used for electrophysiology experiments were human GIRK1 (pGEMSH vector), mouse GIRK2 (pXOOM vector), mouse dopamine D_2 receptor (pXOOM vector), bovine Gβ_1 (pGEMSH vector), bovine Gγ_2 (pGEMSH vector)[75], and human Gα_o, Gα_o^{K46E} or Gα_o^{R209C} (pMAX vector, described above). *Xenopus laevis* oocytes were isolated and microinjected with in vitro synthesized circular RNAs (0.125 to 2.5 ng per oocyte)[76]. To allow for sufficient protein expression, injected oocytes were incubated at 18 °C for 2 days. The following day, a GeneClamp 500 amplifier (Axon Instruments) was used to measure whole-cell oocyte currents. The microelectrodes had resistances of 0.5 to 1 MΩ using a 3 M KCl solution in 1.4% agarose. For TEVC measurements, oocytes were held at 0 mV (E_K), and a ramp protocol with a command potential from −80 to +80 mV was used to monitor the currents. The current amplitude was measured at the end of a sweep of 0.4 s. All currents were analyzed when steady state was reached. To establish a baseline for TEVC recordings, oocytes were perfused with a low K^+ (LK) solution ND96 (2 mM KCl, 96 mM NaCl, 1 mM $MgCl_2$, 1.8 mM $CaCl_2$, 5 mM HEPES–Na pH 7.4). A high potassium (High K +) solution ND96K (96 mM KCl, 10 mM HEPES–K pH 7.4, 1 mM $MgCl_2$, and 1.8 mM $CaCl_2$) was used to measure basal current. The oocyte chamber was perfused with 3 mM $BaCl_2$ (Ba^{2+}) in ND96K to block the current. The barium-sensitive current was used exclusively for statistical analysis. Ten µM dopamine in ND96K was used to determine the effect of Gα_o wild type and mutants on agonist-induced activity of GIRK channels.

Basal and receptor-mediated activation of GIRK1/GIRK2 channels was determined by whole-cell patch-clamp recordings[42,77], HEK293T (ATCC; CRL-1573) cells were maintained in Dulbecco's Modified Eagle Medium (Life Technologies; 11965-118) supplemented with 100 U/mL penicillin, 100 mg/mL streptomycin, and 10% (v/v) heat-inactivated fetal bovine serum (HI-FBS; Thermo Fisher Scientific, 10438026). Lipofectamine 3000 (Thermo Fisher Scientific; L3000015) was used in accordance with the manufacturer's protocol to transiently transfect cDNAs for rodent GIRK1-GIRK2 tandem dimer (200 ng)[77], eYFP (50 ng)[77], human MOR (400 ng)[78], and one of the following Gα_o subunits, human Gα_o, Gα_o^{K64E} or Gα_o^{R209C} (400 ng) (constructs described above). All genes were cloned into pcDNA3 vector. 48-72 h post-transfection, cells were plated onto Matrigel-coated (0.4% v/v) 12 mm glass coverslips (Electron Microscopy Sciences; 72290-03) in 24 well plate (VWR; 10062-896) for whole-cell patch-clamp recordings. Whole-cell recordings were made with the investigator blinded to the Gα type, and then unblinded after completing the recordings.

Whole-cell patch-clamp recordings were acquired using an Axopatch 200B amplifier and pClamp software (Molecular Devices)[42,77]. Whole-cell series resistance compensation was applied and used to measure the cell size (pF). Patch-clamp experiments were conducted in 20 K external solution, containing 10 mM HEPES pH 7.4, 140 mM NaCl, 20 mM KCl, 2 mM $MgCl_2$, 0.5 mM $CaCl_2$ (~318 mOsm). Borosilicate glass electrodes (Warner Instruments) had resistances of 3-4 MΩ and were filled with internal solution containing 10 mM HEPES pH 7.4, 20 mM NaCl, 130 mM KCl, 5.46 mM $MgCl_2$, 5 mM EGTA, 2.56 mM K_2ATP, and 0.3 mM LiGTP (~ 300 mOsm). 10 µM DAMGO, 100 mM PrOH, and 1 mM $BaCl_2$ were prepared in the external solution on the day of the experiment.

Currents were measured (10 kHz sampling and 1 kHz filter) from eYFP-positive cells using a voltage protocol of a holding potential of −40 mV, followed by a 60 ms step to −100 mV and a voltage ramp to 50 mV over 200 ms. Solutions were applied locally for 30 s with a rapid perfusion pipet in the following order: 20 K, 20 K + PrOH, 20 K, 20 K + DAMGO, 20 K, 20 K + $BaCl_2$, and 20 K. The maximal inward current was measured at −100 mV. Except for DAMGO, the average current was calculated during the 30 s drug application. For DAMGO, the maximal inward current was calculated before the onset of MOR desensitization. To adjust for differences in GIRK channel expression, MOR activation was compared to G protein-independent alcohol activation[41], and calculated as a ratio of DAMGO-induced to PrOH-induced currents ($I_{DAMGO} - I_{Basal}$)/($I_{PrOH} - I_{Basal}$). Barium-sensitive inhibition of GIRK current density was calculated as ($I_{Basal} - I_{Ba2+}$)/pF. Cells not expressing a propanol-activated current were excluded from the analysis. Statistical tests performed using one-way ANOVA followed by Dunnett's post hoc test (GraphPad Prism 9.0).

Expression and purification of Gα_o

Bacterial expression was used for the production of recombinant full-length human Gα_o[79,23]. Rosetta (Novagen; 70954) or RIPL (Agilent; 230280) cells were transformed with PET-SUMO-Gα_o (human, wild type and mutant) plasmid (derived from PET-SUMO-Gα_{i1}[79]) and grown at 37 °C in 2X Luria Broth to saturation. Once at OD_{600} = 0.6–0.8, protein expression was induced by adding 600 µM isopropyl-β-D-1-thiogalactoside. The culture temperature was lowered to 16 °C and shaken overnight. The subsequent purification was carried out at 4 °C for all steps. The saturated cell culture was collected by centrifugation at 5400×*g* for 30 min. Cells were lysed by sonication and clarified by centrifugation at 26,900×*g* for 45 min. Lysates (30 mL each) were incubated with 5 mL (10 mL 50/50 slurry) of HisPur™ Ni-NTA Resin (Thermo Fisher Scientific; 88221) or ProBond Ni-chelating resin (Invitrogen; R80101) and 10 mM imidazole for 1 h. The resin was washed twice with phosphate buffer pH 7.0 (25 mM H_2KO_4P, 25 mM HK_2O_4P, 500 mM (tris(2-carboxyethyl)phosphine) (TCEP), 50 µM GDP, 50 µM $MgCl_2$) then twice with phosphate buffer + 10 mM imidazole. Protein was eluted with phosphate buffer + 250 mM imidazole. The SUMO tag was cleaved by addition of 0.5 mg ULP1 protease and the eluate was dialyzed overnight in 4 L of phosphate buffer. The next day, cleaved protein was collected by reverse-nickel chromatography.

Expression and purification of Gβγ

Recombinant baculovirus was used for the production of recombinant rat biotinylated $G\beta_1$[80] and bovine $G\gamma_2$[81], for BLI analysis[81]. Briefly, High 5 cells (Invitrogen; B85502) were grown in SF900 II serum-free medium (Thermo-Fisher; 10902104) in suspension culture at 27 °C with continuous shaking. 2×10^6 cells/mL were infected with high titer $G\beta_1$ and $G\gamma_2$ baculoviruses. After 48 hr the cells were collected by centrifugation at 2600×*g*, resuspended in 50 mL of lysis buffer (50 mM HEPES pH 8.0, 3 mM $MgCl_2$, 50 mM NaCl, 10 mM 2-mercaptoethanol (2-ME), 1 mM EDTA, 50 µM 1 mL/L of protease inhibitor cocktail (Sigma-Aldrich; P-2714), and freeze-thawed using liquid nitrogen four times and maintained after at 4 °C. Samples were then diluted to 100 mL and centrifuged at 50,000 x*g* for 30 min. After discarding the supernatant, the pellet was resuspended in 5 mL membrane wash buffer (50 mM HEPES pH 8.0, 3 mM $MgCl_2$, 50 mM NaCl, 50 µM 1 mL/L of protease inhibitor cocktail, 10 mM 2-ME, 50 µM GDP) and transferred to a dounce homogenizer. Upon resuspension, the volume was brought to 60 mL with additional membrane wash buffer. Using a cholate solution (Sigma-Aldrich; 229101)[82], cholate was added to a final concentration of 1% and allowed to extract for 1 h with stirring. Following cholate extraction, the membranes were centrifuged at 125,000 x*g* for 45 min. The resulting supernatant was diluted to 5 times the initial volume by slowly adding Buffer A (20 mM HEPES pH 8.0, 1 mM $MgCl_2$, 100 mM NaCl, 10 mM 2-ME, 50 µM 1 mL/L of protease inhibitor cocktail, 50 µM GDP, 0.5% Lubrol (C12E10) (Sigma-Aldrich; P9769) to the stirring solution.

The diluted solution was loaded onto a Ni-NTA agarose column (Qiagen; 1018244) equilibrated with Buffer A. The column was then washed with 100 mL Buffer B (20 mM HEPES pH 8.0, 1 mM $MgCl_2$, 300 mM NaCl, 10 mM 2-ME, 50 µM 1 mL/L of protease inhibitor cocktail, 10 mM imidazole, 10 µM GDP, 0.5% lubrol). Following this, the column was warmed tmo room temperature (RT) for 15 min and washed with an additional 8 mL of RT Buffer B. The column was then washed with 32 mL of Buffer C (20 mM HEPES pH 8.0, 100 mM NaCl, 50 mM $MgCl_2$, 10 mM NaF, 30 µM $AlCl_3$, 50 µM 1 mL/L of protease inhibitor cocktail, 20 mM imidazole, 10 µM GDP, 0.5% Lubrol) at room temperature. The column was returned to 4 °C, where it was then washed with 10 mL Buffer D (20 mM HEPES pH 8.0, 50 mM NaCl, 0.5% Lubrol, 50 µM 1 mL/L of protease inhibitor cocktail, 20 mM imidazole). Following this, the column was washed with three column volumes of Buffer D (50 mM imidazole). Finally, 2 mL fractions were eluted from the Ni-NTA column with Buffer D (250 mM imidazole). The purified yield was typically 1 mg of $G\beta_1\gamma_2$/L of cell culture[83].

Thermostability measurements

The fast determination of Quantitative Cysteine Reactivity (fQCR) assay was used to determine T_m values for purified $G\alpha_o$ proteins[43]. Briefly, 10 µL of 30 µM protein, 10 µL of 1 mM GDP or GTPγS, 10 µL of 500 mM 4-fluoro-7-sulfamoylbenzofurazan (ABD-F) cysteine-reactive dye (Abcam; 91366-65-3), and 170 µL phosphate buffer pH 7.0 was added to 12-strip PCR tubes. Samples were subjected to a 40-degree temperature gradient in a Biometra TProfessional Thermocycler for 3 min and fluorescence values were collected on a PHERAstar plate reader (BMG Labtech) at 400 nm excitation, 500 nm emission.

Nucleotide loading and hydrolysis

To measure GTP binding and hydrolysis[45,84], BODIPYFL-GTP (ThermoFisher Scientific, Invitrogen; G12411) (50 nM) equilibrated in hydrolysis buffer (50 mM HEPES pH 7, 10 mM $MgCl_2$, 25 mM NaCl) was combined with purified $G\alpha_o$ protein (3 µM) in a 1 mL cuvette for 60 sec. Fluorescence was measured using a Perkin-Elmer Luminescence Spectrometer (502 nm excitation, 511 nm emission) and analyzed using the FLWinLab software package (Perkin-Elmer).

To measure GTPγ^{35}S binding[39], $G\alpha_o$ was diluted to 1 µM in a 50 mM HEPES pH 8.0, 1 mM EDTA, 0.1% C12 E10 (lubrol), and 1 mM dithiothreitol (DTT) in polypropylene reaction tubes on ice. A blank sample was prepared similarly without $G\alpha_o$. An equal volume of binding mix (50 mM HEPES pH 8.0, 1 mM EDTA, 1 mM DTT, 40 mM $MgCl_2$, 200 mM NaCl, 2 µM GTPγ^{35}S, and 300,000 – 800,000 cpm GTPγ^{35}S) was added to each sample, and placed in a 30 °C circulating water bath for 60 min. After incubation, samples were applied to 0.45 µm nitrocellulose filters under vacuum (Cytiva Protran BA85 Nitrocellulose Blotting Membrane; 10402578). Each sample tube was washed three times with 2 mL wash buffer (20 mM Tris-Cl pH 8.0, 100 mM NaCl, 25 mM $MgCl_2$), applying each wash to the filter. The filter was washed three additional times with 2 mL fresh wash buffer. Filter membranes were air dried and samples measured for ^{35}S activity on a scintillation counter.

Biolayer interferometry

Binding of Gα to Gβγ was determined by Biolayer Interferometry (BLI) using Octet Red96 (Fortebio; 18-5019)[85]. Briefly, purified biotinylated Gβγ (3 mg/mL) was incubated for 15 min with streptavidin biosensors in PBST-NGM (25 mM KPO_4 pH 7.0, 50 mM NaCl, 0.1% Tween, 50 µM GDP + 5 mM $MgCl_2$). Purified $G\alpha_o$ (untagged) was diluted into PBST-NGM and then mixed with Gβγ-loaded sensors for 10 min (association) and then protein-free buffer (dissociation) at 25 °C. Nonspecific binding was measured using biosensors that were exposed to buffer alone. Baseline subtraction and Gβγ loading normalization were done in Excel. Kinetic Analysis was done using GraphPad Prism.

Computational methods

Starting structural models and molecular dynamics simulations. The structural model of monomeric GTP-bound $G\alpha_o$ protein with Mg^{2+} ion was built using the monomeric GTP bound mouse $G\alpha_o$ crystal structure (PDB ID: 3C7K) as template and using the homology modeling method in the Prime module of Maestro software from Schrodinger [https://www.schrodinger.com/products/maestro]. The ligand-free apo-state of the monomeric $G\alpha_o$ protein was obtained by removing GTP from the modeled structure; the Mg^{2+} ion is retained in all the simulations since it plays an important role in G protein activity. Point mutations to generate the structures of $G\alpha_o^{K46E}$ and $G\alpha_o^{R209C}$ were performed using Maestro Biologics suite. The side chain packing was done for all the residues with 5 Å of the mutated residue position including the mutated residues using Maestro Prime suite. All structures were subjected to energy minimization using conjugate gradient method with a convergence cutoff of 0.1 kcal/mol/Å. Input files for molecular dynamics (MD) simulations were generated using CHARMM-GUI[86]. Each monomeric $G\alpha_o$ protein was solvated in explicit TIP3P water molecules in a cubic box (9.5 nm × 9.5 nm × 9.5 nm) with 0.15 M of KCl for maintaining the physiological condition. We used software GROMACS[87] (Version 2021.3) with all-atom CHARMM36 force field[88] to perform MD simulations. MD simulations were performed at 310 K coupled to a temperature bath with a relaxation time of 0.1 ps[89]. Pressure of the systems was calculated with molecular virial and was held constant by a weak coupling to a pressure bath with a relaxation time of 0.5 ps. Equilibrium bond length and geometry of water molecules were constrained using the SHAKE algorithm[90]. The short-range electrostatic and van der Waals interactions were estimated every 2 fs using a charged group pair list with cutoff of 8 Å between centers of geometry of charged groups. Long-range van der Waals interactions were calculated using a cutoff of 14 Å and long-range electrostatic interactions were treated with the particle mesh Ewald method[91]. Temperature was kept constant at 310 K by applying the Nose-Hoover thermostat[92]. Desired pressure for all systems were achieved by using Parrinello-Rahman barostat with a pressure relaxation time of 2 ps[93]. Before production runs, all systems were subjected to a 5000-step steepest descent energy minimization to remove bad contacts[94]. After minimization, the systems were heated up to 310 K under constant temperature-volume ensemble (NVT). The simulations were saved every 200 ps for analysis. The protein, Mg^{2+} ion, and nucleotide were subjected to positional constraints under a harmonic force constant of

1000 kJ/(mol*nm^2) during the NVT step while solvent molecules were free to move. The systems then were further equilibrated using constant pressure ensemble (NPT), in which the force constant applied to the protein, Mg^{2+} ion, and nucleotide were gradually reduced from 5 kJ/(mol*nm^2) to zero in six steps of 5 ns each. An additional 50 ns of unconstrained simulations were performed, making it a total of 80 ns NPT equilibration prior to production runs. We performed five production runs of 1000 ns each using five different initial velocities for every system. Therefore, we had 5 µs long MD trajectory for wild type and K46E monomeric $G\alpha_o$ protein of GTP-bound state or apo state, and 5 µs long MD trajectory for R209C monomeric $G\alpha_o$ protein of GTP-bound state only. The convergence of the MD simulations was ascertained by plotting the RMSD in the coordinates of the Cα atoms as a function of time showing lowering of fluctuations (Supplementary Fig. 2C).

Calculation of residue contact map of protein with nucleotide. For $G\alpha_o^{WT}$ and $G\alpha_o^{K46E}$ systems that contain nucleotide, the last 200 ns from five independent molecular dynamics simulation runs were merged into one concatenated trajectory. The concatenated trajectory was sampled every 2 ns. The sampled trajectory was fed to GetContacts script available on GitHub [https://github.com/getcontacts/getcontacts]. For specific parameters, the interaction type flag "itype" was set to "all", and the two atom group flags for contacts were "protein" and "resname GTP". Contact results were further processed in Python environment: briefly, contacts with van der Waals force were excluded, and contact frequency of every contact was calculated. Contact frequencies between $G\alpha_o^{WT}$ system and $G\alpha_o^{K46E}$ system were compared, and contacts with more than 30% frequency decreases from the $G\alpha_o^{WT}$ system to $G\alpha_o^{K46E}$ system were selected and depicted.

Calculation of interaction energy of nucleotide with the protein. For each system ($G\alpha_o^{WT}$, $G\alpha_o^{K46E}$, and $G\alpha_o^{R209C}$), we aggregated the last 200 ns of each simulation run to calculate the interaction energy of GTP with the $G\alpha_o$ protein. Total non-bond interaction energy (van der Waals + Columbic) between $G\alpha_o$ protein and GTP (shown in Fig. 4G) was calculated using gmx energy module of GROMACS. The interaction energy was calculated for every snapshot and averaged for the last 200 ns in all five simulation runs for every system.

Principal Component Analysis, free energy surface generation, and representative structures. For apo systems of WT and K46E, five full-length independent molecular dynamics simulation runs were merged into one concatenated trajectory. Principal component analysis was performed on each concatenated trajectory using gmx covar module of GROMACS with covariance matrix of Cα atoms of all residues. The first two principal components (PC1 and PC2) of every system were extracted using gmx anaeig module of GROMACS and imported into Python as a data-frame using Python Pandas package. The kernel density value of the data-frame was calculated using Python scikit-learn package. The multiplicative inverse of the kernel density values was used as the Z-axis values to plot the free energy surface. Both the 3-D and 2-D density maps were plotted using Python Matplotlib package. Representative structures of local and global minima were extracted by first clustering the points using K-mean clustering method and extracting cluster centers using K-medoids method from Python scikit-learn package.

Radioligand binding assays

Saturation binding assays were performed using membranes from Expi293™cells (ThermoFisher; A14527) transiently expressing wild-type and mutant MOR-$G\alpha_o$ fusion. Binding assays were set up in 96-well plates in standard binding buffer (50 mM HEPES, pH 7.4, 50 mM NaCl, 20 mM $MgCl_2$, 0.5 mM EDTA, ±100 µM GppCp). Saturation binding assays with 0.5–10 nM [^{3}H]-DAMGO (Perkin-Elmer, specific activity 51.7 Ci/mmol; NET902250UC) in standard binding buffer were performed to determine equilibrium dissociation constant (K_d) and B_{max}, whereas 10 µM final concentration of morphine was used to define nonspecific binding. All reactions were incubated for 1.5 h at room temperature in the dark and terminated by rapid vacuum filtration onto chilled 0.3% PEI-soaked GF/C UniFilter plates (Perkin-Elmer; 6055690) followed by three quick washes with cold washing buffer (50 mM Tris HCl, pH 7.4). The UniFilter plates were dried in an oven before adding 20 µl/well Microscint™-O cocktail (Perkin-Elmer; 6013611). Radioactivity counts were determined using a Wallac Trilux MicroBeta counter in the form of corrected count per min (ccpm) with counting efficiency of 40% (Perkin-Elmer). Results were analyzed using GraphPad Prism 9.0 using "One site -- Total and nonspecific binding". Statistical differences ($p < 0.05$) of pK_d values derived from concentration-response assays were determined by using the Extra sum-of-squares F test ($p < 0.05$) function in GraphPad Prism 9.0 comparing control versus 100 µM GppCp.

Construction and expression of the receptor-G protein complex

The Bac-to-Bac baculovirus expression system (Invitrogen; 10359016) was used to generate the recombinant baculovirus for protein expression. Baculoviruses corresponding to N-terminal Maltose Binding Protein (MBP) - human D_2 receptor (MBP-D2R), human G_{oA}^{K46E}, $G\beta_1\gamma_2$ were co-expressed by infecting Sf9 cells at a density of 2×10^6 cells per mL at MOI ratio of 3:1.5:1.5 ±scFv16 at an MOI of 1, respectively. Cells were harvested by centrifugation at 3500×g for 15 min 48 h post-infection and stored at −80 °C for future use.

Receptor-G protein complex purification

The cell pellet of the D2R-G_{oA}^{K46E} complex was thawed on ice and incubated with 20 mM HEPES pH 7.5, 100 mM NaCl, 20 mM $MgCl_2$, 20 mM KCl, 5 mM $CaCl_2$, proteinase inhibitor, 40 units apyrase, 50 µM dopamine, and 100 µM TCEP at room temperature. After 1.5 h, the cell suspension was homogenized, membrane was collected by centrifugation at 100,000×g for 35 min and solubilized using 20 mM HEPES pH 7.5, 100 mM NaCl, 10% (w/v) glycerol, 0.5% (w/v) lauryl maltose neopentyl glycol (LMNG, Anatrace; NG310), 0.05% (w/v) cholesteryl hemisuccinate (CHS), 20 mM $MgCl_2$, 20 mM KCl, 5 mM $CaCl_2$, proteinase inhibitor, 40 units apyrase, 50 µM dopamine, and 100 µM TCEP for 4 h at 4 °C. The solubilized proteins were isolated by ultracentrifugation at 100,000×g for 45 min and then incubated overnight at 4 °C with TALON IMAC resin (Takara; 635653) and 20 mM imidazole. The resin was collected the next day and washed with 25 column volumes 20 mM HEPES pH 7.5, 100 mM NaCl, 20 mM imidazole, 0.01% (w/v) LMNG, 0.001% (w/v) CHS, 50 µM dopamine, and 100 µM TCEP. The protein was then eluted using the same buffer supplemented with 250 mM imidazole. Eluted protein was subjected to TEV protease (in-house) overnight at 4 °C and a ratio of 1:10 (1 mg receptor: 0.1 mg TEV). The protein was then concentrated and subjected to size-exclusion chromatography on a Superdex 200 Increase 10/300 column (GE Healthcare; 289909944) that was pre-equilibrated with 20 mM HEPES pH 7.5, 100 mM NaCl, 20 mM $MgCl_2$, 50 µM dopamine, 0.00075% (w/v) LMNG, 0.00025 (w/v) glyco-diosgenin (GDN, Anatrace; GDN101), 0.00075% (w/v) CHS, and 100 µM TCEP. Peak fractions were pooled and concentrated to 5 mg/mL for making of cryoEM grids. For complex formation in the presence of ATP/GTP the above protocol was followed without apyrase. Complexes were also subjected to purification after the TALON column using an Anti-flag column (Genscript; L00432) and eluted with 500 µg/mL Flag peptide (Genscript; RP10586) prior to TEV cleavage and S200 column.

CryoEM data collection, 3D reconstitution, model building and refinement

For cryo-EM data collection and processing of the D2R-G_{oA}^{K46E} complex[95], samples (3.2 µl) were applied to glow-discharged Quantifoil

R1.2/1.3 Au300 holey carbon grids (Ted Pella; 658-300-AU) individually and were flash-frozen in a liquid ethane/propane (40/60) mixture using a Vitrobot Mark IV (FEI) set at 4 °C and 100% humidity with a blot time range from 3.0 to 4.5 sec. Images were collected using a 200 keV Talos Artica with a Gatan K3 direct electron detector at a physical pixel size of 0.88 Å. Micrograph recorded movies were automatically collected using SerialEM using a multishot array[96]. Data were collected at an exposure dose rate of ~15 electrons/pixel/sec as recorded from counting mode. Images were recorded for ~1.7–2.7 s in 60 subframes to give a total exposure dose of ~45 electrons per Å^2. Following manual inspection and curation of the micrographs, particles were selected using the Blob particle picker and initial 2D classification yielded templates for subsequent template picking. After one round of two-dimensional classification and selection in cryoSPARC, a subset of the selected particles was used as a training set for Topaz and the particles were re-picked from the micrographs using Topaz[97] and subjected to two-dimensional classification and three-dimensional classification. The select classified picked particle coordinates were next merged yielding a subset of unique particles that survived 2D classification (i.e. duplicates were removed with a radius of 25 pixels). All subsequent three-dimensional classification and refinement steps were performed within cryoSPARC[98]. Multiple rounds of multi-terence refinement resolved the final stack of particles that produced a map with a resolution reported in Supplementary Table 1 (by FSC using the 0.143 Å cut-off criterion)[99] after Global CTF refinement and post-processing including soft masking, B-factor sharpening in cryoSPARC to generate the post-processed sharpened map. Alternative post-sharpening was performed on the two half-maps using deepEMhancer[100]. For more details see Supplementary Table 1.

Maps from deepEMhancer were used for map building, refinement, and subsequent structural interpretation. The D2R cryo-EM structure (PDB ID: 8IRS) was used as the initial model and docked into the cryo-EM map using Chimera[101] followed by initial rigid body and simulated annealing then iterative manual adjustment in COOT[102] and Phenix.real_space_refine in Phenix[103]. A composite map was generated by merging two local refines maps, one for the AHD domain and one for the entire complex, via the Chimera. This composite map displayed main and side chain densities for most part, which enabled placing of the all helical domain. The final refined model for the full D2R-Gα_o^{K46E} complex also matches the consensus map. Model statistics were validated using Molprobity. Structural figures were prepared using Chimera or Pymol [https://pymol.org/2/]. Coordinates of D2R complexes and EM maps have been deposited in the Protein Data Bank and the Electron Microscopy Data Bank under the accession codes 8U02 (EMD-41776 and 8TZQ EMD-41766) for the DR2-Gα_o^{K46E} and DR2-Gα_{oA}^{K46E}-scFv16, respectively. Interface analysis was accomplished using Contact and Areaimol of the CCP4 Suite[104] along with the PISA Server[105] [http://www.ebi.ac.uk/pdbe/prot_int/pistart.html].

Reporting summary

Further information on research design is available in the Nature Portfolio Reporting Summary linked to this article.

Data availability

Complete sequences for plasmids generated in this study are provided in Supplementary Information: PET-SUMO-Gα_o for purification, pMAX-Gα_o for GIRK assays in *X. oocyes*, pcDNA3.1-Gα_o for GIRK assays in HEK293 cells, MOR-Gα_o fusion for radioligand binding, and pFastbac-Gα_o for cryo-electron microscopy. Cryo-EM density maps have been deposited in the Electron Microscopy Data Bank under accession codes 8U02 and EMD-41776 for the DR2-Gα_o^{K46E}, and 8TZQ and EMD-41766 for DR2-Gα_{oA}^{K46E}-scFv16. Source data supporting Fig. 2 (BRET), Fig. 3 (potassium current), Fig. 4A and B (thermostability), Fig. 4C (BODIPY fluorescence), Fig. 4D (radiolabeled GTP binding), Fig. 4E (BLI), Fig. 4F (Principal Component analysis), and Fig. 5A–C (radioligand binding) are provided with this paper. Source data are provided with this paper.

References

1. Flock, T. et al. Universal allosteric mechanism for Galpha activation by GPCRs. *Nature* **524**, 173–179 (2015).
2. Flock, T. et al. Selectivity determinants of GPCR-G-protein binding. *Nature* **545**, 317–322 (2017).
3. Sprang, S. R. Invited review: activation of G proteins by GTP and the mechanism of Gα-catalyzed GTP hydrolysis. *Biopolymers* **105**, 449–462 (2016).
4. Hilger, D., Masureel, M. & Kobilka, B. K. Structure and dynamics of GPCR signaling complexes. *Nat. Struct. Mol. Biol.* **25**, 4–12 (2018).
5. Muralidharan, K., Van Camp, M. M. & Lyon, A. M. Structure and regulation of phospholipase Cβ and ε at the membrane. *Chem. Phys. Lipids* **235**, 105050 (2021).
6. Halls, M. L. & Cooper, D. M. F. Adenylyl cyclase signalling complexes - pharmacological challenges and opportunities. *Pharm. Ther.* **172**, 171–180 (2017).
7. Smrcka, A. V. & Fisher, I. G-protein βγ subunits as multi-functional scaffolds and transducers in G-protein-coupled receptor signaling. *Cell Mol. Life Sci.* **76**, 4447–4459 (2019).
8. Maguire, M. E., Van Arsdale, P. M. & Gilman, A. G. An agonist-specific effect of guanine nucleotides on binding to the beta adrenergic receptor. *Mol. Pharmacol.* **12**, 335–339 (1976).
9. De Lean, A., Stadel, J. M. & Lefkowitz, R. J. A ternary complex model explains the agonist-specific binding properties of the adenylate cyclase-coupled beta-adrenergic receptor. *J. Biol. Chem.* **255**, 7108–7117 (1980).
10. Kwok-Keung Fung, B. & Stryer, L. Photolyzed rhodopsin catalyzes the exchange of GTP for bound GDP in retinal rod outer segments. *Proc. Natl Acad. Sci. USA* **77**, 2500–2504 (1980).
11. Oldham, W. M., Van Eps, N., Preininger, A. M., Hubbell, W. L. & Hamm, H. E. Mechanism of the receptor-catalyzed activation of heterotrimeric G proteins. *Nat. Struct. Mol. Biol.* **13**, 772–777 (2006).
12. Liu, X. et al. Structural insights into the process of GPCR-G protein complex formation. *Cell* **177**, 1243–1251.e1212 (2019).
13. Van Eps, N. et al. Interaction of a G protein with an activated receptor opens the interdomain interface in the alpha subunit. *Proc. Natl Acad. Sci. USA* **108**, 9420–9424 (2011).
14. Dror, R. O. et al. Structural basis for nucleotide exchange in heterotrimeric G proteins. *Science* **348**, 1361–1365 (2015).
15. Chung, K. Y. et al. Conformational changes in the G protein Gs induced by the beta2 adrenergic receptor. *Nature* **477**, 611–615 (2011).
16. Westfield, G. H. et al. Structural flexibility of the G alpha s alpha-helical domain in the beta2-adrenoceptor Gs complex. *Proc. Natl Acad. Sci. USA* **108**, 16086–16091 (2011).
17. Rasmussen, S. G. et al. Crystal structure of the beta2 adrenergic receptor-Gs protein complex. *Nature* **477**, 549–555 (2011).
18. Kaya, A. I. et al. A conserved hydrophobic core in Gαi1 regulates g protein activation and release from activated receptor. *J. Biol. Chem.* **291**, 19674–19686 (2016).
19. Nehmé, R. et al. Mini-G proteins: novel tools for studying GPCRs in their active conformation. *PLoS ONE* **12**, e0175642 (2017).
20. Jang, W., Lu, S., Xu, X., Wu, G. & Lambert, N. A. The role of G protein conformation in receptor-G protein selectivity. *Nat. Chem. Biol.* **19**, 687–694 (2023).
21. Landis, C. A. et al. GTPase inhibiting mutations activate the alpha chain of Gs and stimulate adenylyl cyclase in human pituitary tumours. *Nature* **340**, 692–696 (1989).
22. Graziano, M. P. & Gilman, A. G. Synthesis in Escherichia coli of GTPase-deficient mutants of Gs alpha. *J. Biol. Chem.* **264**, 15475–15482 (1989).

23. Hewitt, N. et al. Catalytic site mutations confer multiple states of G protein activation. *Sci. Signal* **16**, eabq7842 (2023).
24. Knight, K. M. et al. A universal allosteric mechanism for G protein activation. *Mol. Cell* **81**, 1384–1396.e1386 (2021).
25. Knight, K. M. et al. Molecular annotation of G protein variants in a neurological disorder. *Cell Rep.* **42**, 113462 (2023).
26. Slepak, V. Z. et al. Random mutagenesis of G protein alpha subunit G(o)alpha. Mutations altering nucleotide binding. *J. Biol. Chem.* **268**, 21889–21894 (1993).
27. Apanovitch, D. M., Iiri, T., Karasawa, T., Bourne, H. R. & Dohlman, H. G. Second site suppressor mutations of a GTPase-deficient G-protein a- subunit. Selective inhibition of bg-mediated signaling. *J. Biol. Chem.* **273**, 28597–28602 (1998).
28. Vetter, I. R. & Wittinghofer, A. The guanine nucleotide-binding switch in three dimensions. *Science* **294**, 1299–1304 (2001).
29. Herskowitz, I. Functional inactivation of genes by dominant negative mutations. *Nature* **329**, 219–222 (1987).
30. Barren, B. & Artemyev, N. O. Mechanisms of dominant negative G-protein alpha subunits. *J. Neurosci. Res.* **85**, 3505–3514 (2007).
31. Olsen, R. H. J. et al. TRUPATH, an open-source biosensor platform for interrogating the GPCR transducerome. *Nat. Chem. Biol.* https://doi.org/10.1038/s41589-020-0535-8 (2020).
32. Farfel, Z. et al. Pseudohypoparathyroidism, a novel mutation in the betagamma-contact region of Gsalpha impairs receptor stimulation. *J. Biol. Chem.* **271**, 19653–19655 (1996).
33. Iiri, T., Farfel, Z. & Bourne, H. R. Conditional activation defect of a human Gsalpha mutant. *Proc. Natl Acad. Sci. USA* **94**, 5656–5661 (1997).
34. Hollins, B., Kuravi, S., Digby, G. J. & Lambert, N. A. The c-terminus of GRK3 indicates rapid dissociation of G protein heterotrimers. *Cell Signal* **21**, 1015–1021 (2009).
35. Lambert, N. A. et al. Regulators of G-protein signaling accelerate GPCR signaling kinetics and govern sensitivity solely by accelerating GTPase activity. *Proc. Natl Acad. Sci. USA* **107**, 7066–7071 (2010).
36. Masuho, I. et al. Distinct profiles of functional discrimination among G proteins determine the actions of G protein-coupled receptors. *Sci. Signal.* **8**, ra123 (2015).
37. Muntean, B. S. et al. Gαo is a major determinant of cAMP signaling in the pathophysiology of movement disorders. *Cell Rep.* **34**, 108718 (2021).
38. Yang, X. et al. Phenotypes of GNAO1 variants in a Chinese cohort *Front. Neurol.* **12**, 662162 (2021).
39. Sternweis, P. C. & Robishaw, J. D. Isolation of two proteins with high affinity for guanine nucleotides from membranes of bovine brain. *J. Biol. Chem.* **259**, 13806–13813 (1984).
40. Huff, R. M., Axton, J. M. & Neer, E. J. Physical and immunological characterization of a guanine nucleotide- binding protein purified from bovine cerebral cortex. *J. Biol. Chem.* **260**, 10864–10871 (1985).
41. Aryal, P., Dvir, H., Choe, S. & Slesinger, P. A. A discrete alcohol pocket involved in GIRK channel activation. *Nat. Neurosci.* **12**, 988–995 (2009).
42. Bodhinathan, K. & Slesinger, P. A. Molecular mechanism underlying ethanol activation of G-protein-gated inwardly rectifying potassium channels. *Proc. Natl Acad. Sci. USA* **110**, 18309–18314 (2013).
43. Isom, D. G. et al. Protons as second messenger regulators of G protein signaling. *Mol. Cell* **51**, 531–538 (2013).
44. Goricanec, D. et al. Conformational dynamics of a G-protein alpha subunit is tightly regulated by nucleotide binding. *Proc. Natl Acad. Sci. USA* **113**, E3629–E3638 (2016).
45. McEwen, D. P., Gee, K. R., Kang, H. C. & Neubig, R. R. Fluorescent BODIPY-GTP analogs: real-time measurement of nucleotide binding to G proteins. *Anal. Biochem.* **291**, 109–117 (2001).
46. Willard, F. S., Kimple, A. J., Johnston, C. A. & Siderovski, D. P. A direct fluorescence-based assay for RGS domain GTPase accelerating activity. *Anal. Biochem.* **340**, 341–351 (2005).
47. DeVree, B. T. et al. Allosteric coupling from G protein to the agonist-binding pocket in GPCRs. *Nature* **535**, 182–186 (2016).
48. Maeda, S. et al. Development of an antibody fragment that stabilizes GPCR/G-protein complexes. *Nat. Commun.* https://doi.org/10.1038/s41467-018-06002-w (2018).
49. Zhang, M. et al. Cryo-EM structure of an activated GPCR-G protein complex in lipid nanodiscs. *Nat. Struct. Mol. Biol.* **28**, 258–267 (2021).
50. Wall, M. A. et al. The structure of the G protein heterotrimer Gi alpha 1 beta 1 gamma 2. *Cell* **83**, 1047–1058 (1995).
51. Hilger, D. The role of structural dynamics in GPCR-mediated signaling. *FEBS J.* **288**, 2461–2489 (2021).
52. Huang, W. et al. Structural insights into μ-opioid receptor activation. *Nature* **524**, 315–321 (2015).
53. Filipek, S. Molecular switches in GPCRs. *Curr. Opin. Struct. Biol.* **55**, 114–120 (2019).
54. Wang, S. et al. Structure of the D2 dopamine receptor bound to the atypical antipsychotic drug risperidone. *Nature* **555**, 269–273 (2018).
55. Ferguson, K. M., Higashijima, T., Smigel, M. D. & Gilman, A. G. The influence of bound GDP on the kinetics of guanine nucleotide binding to G proteins. *J. Biol. Chem.* **261**, 7393–7399 (1986).
56. Draper-Joyce, C. J. et al. Structure of the adenosine-bound human adenosine A1 receptor-Gi complex. *Nature* **558**, 559–563 (2018).
57. Liang, Y. L. et al. Phase-plate cryo-EM structure of a biased agonist-bound human GLP-1 receptor-Gs complex. *Nature* **555**, 121–125 (2018).
58. Iiri, T., Bell, S. M., Baranski, T. J., Fujita, T. & Bourne, H. R. A Gsalpha mutant designed to inhibit receptor signaling through Gs. *Proc. Natl Acad. Sci. USA* **96**, 499–504 (1999).
59. Berlot, C. H. A highly effective dominant negative alpha s construct containing mutations that affect distinct functions inhibits multiple Gs-coupled receptor signaling pathways. *J. Biol. Chem.* **277**, 21080–21085 (2002).
60. Wacker, D., Stevens, R. C. & Roth, B. L. How ligands illuminate GPCR molecular pharmacology. *Cell* **170**, 414–427 (2017).
61. Galosi, S. et al. Motor, epileptic, and developmental phenotypes in genetic disorders affecting G protein coupled receptors-cAMP signaling. *Front. Neurol.* **13**, 886751 (2022).
62. Nakamura, K. et al. De Novo mutations in GNAO1, encoding a Gαo subunit of heterotrimeric G proteins, cause epileptic encephalopathy. *Am. J. Hum. Genet.* **93**, 496–505 (2013).
63. Larasati, Y. A. et al. Restoration of the GTPase activity and cellular interactions of Gα. *Sci. Adv.* **8**, eabn9350 (2022).
64. Feng, H. et al. Movement disorder in GNAO1 encephalopathy associated with gain-of-function mutations. *Neurology* **89**, 762–770 (2017).
65. Saitsu, H. et al. Phenotypic spectrum of GNAO1 variants: epileptic encephalopathy to involuntary movements with severe developmental delay. *Eur. J. Hum. Genet.* **24**, 129–134 (2016).
66. Domínguez-Carral, J. et al. Severity of GNAO1-related disorder correlates with changes in g-protein function. *Ann. Neurol.* **94**, 987–1004 (2023).
67. Nishimura, A. et al. Structural basis for the specific inhibition of heterotrimeric Gq protein by a small molecule. *Proc. Natl Acad. Sci. USA* **107**, 13666–13671 (2010).
68. Takasaki, J. et al. A novel Galphaq/11-selective inhibitor. *J. Biol. Chem.* **279**, 47438–47445 (2004).
69. Schrage, R. et al. The experimental power of FR900359 to study Gq-regulated biological processes. *Nat. Commun.* **6**, 10156 (2015).
70. Xiong, X. F. et al. Total synthesis and structure-activity relationship studies of a series of selective G protein inhibitors. *Nat. Chem.* **8**, 1035–1041 (2016).

71. Dai, S. A. et al. State-selective modulation of heterotrimeric Gαs signaling with macrocyclic peptides. *Cell* **185**, 3950–3965.e3925 (2022).
72. Xu, Y. et al. The small molecule GAT1508 activates brain-specific GIRK1/2 channel heteromers and facilitates conditioned fear extinction in rodents. *J. Biol. Chem.* **295**, 3614–3634 (2020).
73. Celver, J., Sharma, M. & Kovoor, A. D(2)-Dopamine receptors target regulator of G protein signaling 9-2 to detergent-resistant membrane fractions. *J. Neurochem.* **120**, 56–69 (2012).
74. Hauser, A. S. et al. Pharmacogenomics of GPCR drug targets. *Cell* **172**, 41–54.e19 (2018).
75. He, C., Zhang, H., Mirshahi, T. & Logothetis, D. E. Identification of a potassium channel site that interacts with G protein betagamma subunits to mediate agonist-induced signaling. *J. Biol. Chem.* **274**, 12517–12524 (1999).
76. Chan, K. W., Sui, J. L., Vivaudou, M. & Logothetis, D. E. Control of channel activity through a unique amino acid residue of a G protein-gated inwardly rectifying K+ channel subunit. *Proc. Natl Acad. Sci. USA* **93**, 14193–14198 (1996).
77. Horvath, G. A. et al. Gain-of-function KCNJ6 mutation in a severe hyperkinetic movement disorder phenotype. *Neuroscience* **384**, 152–164 (2018).
78. Mutneja, M., Berton, F., Suen, K. F., Lüscher, C. & Slesinger, P. A. Endogenous RGS proteins enhance acute desensitization of GABA(B) receptor-activated GIRK currents in HEK-293T cells. *Pflug. Arch.* **450**, 61–73 (2005).
79. Maly, J. & Crowhurst, K. A. Expression, purification and preliminary NMR characterization of isotopically labeled wild-type human heterotrimeric G protein alphai1. *Protein Expr. Purif.* **84**, 255–264 (2012).
80. Ghosh, M., Peterson, Y. K., Lanier, S. M. & Smrcka, A. V. Receptor- and nucleotide exchange-independent mechanisms for promoting G protein subunit dissociation. *J. Biol. Chem.* **278**, 34747–34750 (2003).
81. Kozasa, T. & Gilman, A. G. Purification of recombinant G proteins from Sf9 cells by hexahistidine tagging of associated subunits. Characterization of alpha 12 and inhibition of adenylyl cyclase by alpha z. *J. Biol. Chem.* **270**, 1734–1741 (1995).
82. Tanabe, S., Kreutz, B., Suzuki, N. & Kozasa, T. Regulation of RGS-RhoGEFs by Galpha12 and Galpha13 proteins. *Methods Enzymol.* **390**, 285–294 (2004).
83. Kozasa, T. & Gilman, A. G. Protein kinase C phosphorylates G12 alpha and inhibits its interaction with G beta gamma. *J. Biol. Chem.* **271**, 12562–12567 (1996).
84. Jones, J. C., Jones, A. M., Temple, B. R. & Dohlman, H. G. Differences in intradomain and interdomain motion confer distinct activation properties to structurally similar Gα proteins. *Proc. Natl Acad. Sci. USA* **109**, 7275–7279 (2012).
85. Seneviratne, A. M., Burroughs, M., Giralt, E. & Smrcka, A. V. Direct-reversible binding of small molecules to G protein betagamma subunits. *Biochim. Biophys. Acta* **1814**, 1210–1218 (2011).
86. Jo, S., Kim, T., Iyer, V. G. & Im, W. CHARMM-GUI: a web-based graphical user interface for CHARMM. *J. Comput. Chem.* **29**, 1859–1865 (2008).
87. Hess, B., Kutzner, C., van der Spoel, D. & Lindahl, E. GROMACS 4: algorithms for highly efficient, load-balanced, and scalable molecular simulation. *J. Chem. Theory Comput.* **4**, 435–447 (2008).
88. Huang, J. et al. CHARMM36m: an improved force field for folded and intrinsically disordered proteins. *Nat. Methods* **14**, 71–73 (2017).
89. Berendsen, H. J. C., Postma, J. P. M., Gunsteren, W. F. V., DiNola, A. & Haak, J. R. Molecular dynamics with coupling to an external bath. *J. Chem. Phys.* **81**, 3684–3690 (1984).
90. Andersen, H. C. Rattle: a "velocity" version of the shake algorithm for molecular dynamics calculations. *J. Comput. Phys.* **52**, 24–34 (1983).
91. Darden, T., York, D. & Pedersen, L. Particle mesh Ewald: an N·log(N) method for Ewald sums in large systems. *J. Chem. Phys.* **98**, 10089–10092 (1993).
92. Evans, D. J. & Holian, B. L. The Nose–Hoover thermostat. *J. Chem. Phys.* **83**, 4069–4074 (1985).
93. Parrinello, M. & Rahman, A. Polymorphic transitions in single crystals: A new molecular dynamics method. *J. Appl. Phys.* **52**, 7182–7190 (1981).
94. Petrova, S. S. & Solov'ev, A. D. The origin of the method of steepest descent. *Historia Math.* **24**, 361–375 (1997).
95. Peck, J. V., Fay, J. F. & Strauss, J. D. High-speed high-resolution data collection on a 200 keV cryo-TEM. *IUCrJ* **9**, 243–252 (2022).
96. Mastronarde, D. N. Automated electron microscope tomography using robust prediction of specimen movements. *J. Struct. Biol.* **152**, 36–51 (2005).
97. Bepler, T., Kelley, K., Noble, A. J. & Berger, B. Topaz-Denoise: general deep denoising models for cryoEM and cryoET. *Nat. Commun.* **11**, 5208 (2020).
98. Punjani, A., Zhang, H. & Fleet, D. J. Non-uniform refinement: adaptive regularization improves single-particle cryo-EM reconstruction. *Nat. Methods* **17**, 1214–1221 (2020).
99. Rosenthal, P. B. & Henderson, R. Optimal determination of particle orientation, absolute hand, and contrast loss in single-particle electron cryomicroscopy. *J. Mol. Biol.* **333**, 721–745 (2003).
100. Sanchez-Garcia, R. et al. DeepEMhancer: a deep learning solution for cryo-EM volume post-processing. *Commun. Biol.* **4**, 874 (2021).
101. Pettersen, E. F. et al. UCSF Chimera–a visualization system for exploratory research and analysis. *J. Comput Chem.* **25**, 1605–1612 (2004).
102. Emsley, P. & Cowtan, K. Coot: model-building tools for molecular graphics. *Acta Crystallogr. D Biol. Crystallogr.* **60**, 2126–2132 (2004).
103. Adams, P. D. et al. PHENIX: a comprehensive Python-based system for macromolecular structure solution. *Acta Crystallogr. D Biol. Crystallogr.* **66**, 213–221 (2010).
104. Potterton, E., Briggs, P., Turkenburg, M. & Dodson, E. A graphical user interface to the CCP4 program suite. *Acta Crystallogr. D Biol. Crystallogr.* **59**, 1131–1137 (2003).
105. Krissinel, E. & Henrick, K. Inference of macromolecular assemblies from crystalline state. *J. Mol. Biol.* **372**, 774–797 (2007).

Acknowledgements

Funded by NIH grants F32NS124758 (W.G.L.), F31AA027949 (I.P.), R01GM117923 and R01LM013876 (N.V.), R35GM127303 (A.V.S.), R01AA018734 and U10AA008401 (P.A.S.), R01HL059949 (D.E.L.), RO1DA036596 (K.A.M.), R01MH112205 (B.L.R.), and R35GM118105 (H.G.D). The authors wish to thank Emily Brinson and Harris Teeter for motivating the GIRK channel work.

Author contributions

K.M.K., B.E.K., N.J.K., W.G.L., M.C., S.M., I.P., E.G.O., T.J.L., W.W., N.M., X-P.H., J.F.F., N.V., A.V.S., P.A.S., D.E.L., K.A.M., B.L.R., and H.G.D.: conceptualization. K.M.K., B.E.K., N.J.K., W.G.L., M.C., S.M., I.P., E.G.O., T.J.L., W.W., N.M., X-P.H., J.F.F., N.V., A.V.S., P.A.S., D.E.L., K.A.M., B.L.R., and H.G.D.: formal analysis. W.G.L., I.P., N.V., A.V.S., P.A.S., D.E.L., K.A.M., B.L.R., and H.G.D.: funding acquisition. K.M.K., B.E.K., N.J.K., W.G.L., M.C., S.M., I.P., E.G.O., T.J.L., W.W., N.M., X-P.H., and J.F.F.: investigation. N.V., A.V.S., P.A.S., D.E.L., K.A.M., B.L.R., and H.G.D.: project administration. N.V., A.V.S., P.A.S., D.E.L., K.A.M., B.L.R., and H.G.D.: Supervision. K.M.K., B.E.K., N.J.K., W.G.L., M.C., S.M., I.P., E.G.O., T.J.L., W.W., N.M., X-P.H., J.F.F., N.V., A.V.S., P.A.S., D.E.L., K.A.M., B.L.R., and H.G.D.: validation. K.M.K., B.E.K., N.J.K., W.G.L., M.C., S.M., I.P., E.G.O., T.J.L., W.W., N.M., X-P.H., J.F.F., N.V., A.V.S., P.A.S., D.E.L., K.A.M., B.L.R., and H.G.D.: writing – original draft. K.M.K. and H.G.D.: writing – review & editing

Competing interests

B.L.R. is an SAB member of Escient, Septerna and Lassogen and UNC has licensed technology from his lab to many biotechnology and pharmaceutical companies. The remaining authors declare no competing interests.

Additional information

Supplementary information The online version contains supplementary material available at https://doi.org/10.1038/s41467-024-50964-z.

Correspondence and requests for materials should be addressed to Henrik G. Dohlman.

Peer review information *Nature Communications* thanks Moritz Bunemann, Qiuyan Chen, Francesco Raimondi and the other, anonymous, reviewer(s) for their contribution to the peer review of this work. A peer review file is available.